Title: A descending inhibitory mechanism of nociception mediated by an evolutionarily conserved neuropeptide system in *Drosophila*

Authors: Izumi Oikawa[1], Shu Kondo[2], Kao Hashimoto[3], Akiho Kashiwabara[1], Hiromu Tanimoto[4], Katsuo Furukubo-Tokunaga[5], Ken Honjo[5, 6*]

Affiliations

[1]Graduate School of Life and Environmental Sciences, University of Tsukuba, Tsukuba, Ibaraki 305-8572, Japan.

[2]Faculty of Advanced Engineering, Tokyo University of Science, Katsushika-ku, Tokyo 125-8585, Japan.

[3]College of Life and Environmental Sciences, University of Tsukuba, Tsukuba, Ibaraki 305-8572, Japan.

[4]Graduate School of Life Sciences, Tohoku University, Sendai, Miyagi 980-8577, Japan.

[5]Faculty of Life and Environmental Sciences, University of Tsukuba, Tsukuba, Ibaraki 305-8572, Japan.

[6]Center for Development of Advanced Medicine for Dementia, National Center for Geriatrics and Gerontology, Obu, Aichi 474-8511, Japan.

*Correspondence: Ken Honjo (khonjo@ncgg.go.jp, khonjo831@gmail.com)

Abstract

Nociception is a neural process that animals have developed to avoid potentially tissue-damaging stimuli. While nociception is triggered in the peripheral nervous system, its modulation by the central nervous system is a critical process in mammals, whose dysfunction has been extensively implicated in chronic pain pathogenesis. The peripheral mechanisms of nociception are largely conserved across the animal kingdom. However, it is unclear whether the brain-mediated modulation is also conserved in non-mammalian species. Here, we show that *Drosophila* has a descending inhibitory mechanism of nociception from the brain, mediated by the neuropeptide Drosulfakinin (DSK), a homolog of cholecystokinin (CCK) that plays an important role in the descending control of nociception in mammals. We found that mutants lacking *dsk* or its receptors are hypersensitive to noxious heat. Through a combination of genetic, behavioral, histological, and Ca^{2+} imaging analyses, we subsequently revealed neurons involved in DSK-mediated nociceptive regulation at a single-cell resolution and identified a DSKergic descending pathway that inhibits nociception. This study provides the first evidence for a descending modulatory mechanism of nociception from the brain in a non-mammalian species that is mediated by the evolutionarily conserved CCK system, raising the possibility that the descending inhibition is an ancient mechanism to regulate nociception.

Introduction

Minimizing tissue damage is a fundamental task for all animals to increase their chance of survival. Thus, elucidating the principles of nociception, the neural process detecting and encoding potentially tissue-damaging stimuli, is critical to understanding the molecular and neural mechanisms implementing adaptive behaviors and their evolution. Nociceptors are sensory neurons specialized to detect harmful stimuli, whose activation triggers downstream nociceptive circuits and nocifensive responses[1]. Since the activities of nociceptors and downstream nociceptive circuits are tightly linked to pain perception in humans, unveiling the mechanisms of nociception is also crucial to a better understanding of human pain mechanisms[2, 3].

Descending inhibition has been suggested to be a pivotal mechanism in the modulation of nociception and pain in mammals. Since the discovery that electrical stimulations of parts of the midbrain in rats enabled surgical operations without anesthetics[4], mammalian descending nociceptive pathways have been implicated in various analgesic phenomena/treatments and the development of chronic pain states, suggesting their critical role in modulating nociception and pain[5, 6]. However, brain-mediated modulatory mechanisms of nociception such as descending inhibition have currently been identified only in mammals, despite a high degree of commonality across species in the peripheral nociceptive mechanisms[7, 8]. Therefore, it is unknown whether the descending modulation is a *de novo* mechanism typical of the highly developed mammalian central nervous system (CNS) or a conserved control also present in simpler animals.

The descending nociceptive-modulatory systems in mammals have been revealed to involve various

neurochemical pathways[5, 6, 9]; among these, the cholecystokinin (CCK) system is one of the most extensively characterized[6, 9]. In rodents, CCK signaling plays a crucial role in facilitating nociception by counteracting the opioidergic systems in the periaqueductal gray (PAG)—rostral ventral medulla (RVM)—spinal descending pathway[10-13] and inhibiting nociception through the central amygdala (CeA)—PAG—spinal pathway[14]. In humans, CCK signaling has been implicated in nocebo hyperalgesia, mediated by the descending nociceptive control system[15]. The CCK system is very well-conserved and has been implicated in several common physiological functions among bilaterian species[16-20]. However, whether CCK is functionally involved in regulating nociception outside of mammals remains unknown.

Drosulfakinin (DSK), a neuropeptide homologous to CCK, was identified in the fruit fly *Drosophila melanogaster*[19]. Fly DSK is reportedly involved in modulating many physiological functions shared with mammals, including gut functions, anxiety, aggression, memory, feeding, synaptic functions, and courtship behaviors[19, 21-23]. After the discovery of stereotyped nociceptive escape behavior called rolling and polymodal Class IV md (C4da) nociceptors[24, 25], the larval *Drosophila* has been successfully utilized to identify evolutionarily conserved and previously uncharacterized molecular pathways in nociception[26-34]. The relatively simple architecture of *Drosophila* larvae has also served as an attractive system to elucidate circuitry mechanisms in the ventral nerve cord (VNC; the invertebrate equivalent of the spinal cord) to compute multimodal sensory stimuli and select nociceptive escape strategies[35-40]. Previous studies have demonstrated that neuropeptidergic systems also participate in regulating nociception in *Drosophila*[39, 41-44]. However, the role of fly DSK in nociception remains elusive.

Here, using a collective approach of genetic, behavioral, histological, and Ca^{2+} imaging analyses, we pursued the mechanisms of DSK-mediated nociceptive regulation and demonstrate that the DSK system constitutes a descending inhibitory pathway of nociception from the brain to the VNC in larval *Drosophila*.

Results

DSK signaling negatively regulates thermal nociception

Through a thermal nociception screen using the nocifensive rolling response of *Drosophila* larvae, we found that a deletion mutant line of the *dsk* gene showed thermal hypersensitivity with a significantly shorter latency in their response to a 42 °C probe than the controls, suggesting that DSK plays a role in negatively regulating nociception (Fig. 1A and B). A genomic fragment containing the wild-type *dsk* gene, and no other neuropeptide genes, significantly rescued the thermal hypersensitivity of the *dsk* mutants (Fig. 1B), confirming that *dsk* is responsible for the thermal hypersensitivity.

DSK has been shown to activate two G-protein coupled receptors, CCKLR-17D1 and CCKLR-17D3[45, 46], which are orthologous to the mammalian CCK receptors, CCKAR (also known as CCK_1) and CCKBR (also known as CCK_2)[16-18]. To test whether these receptors mediate DSK signaling in nociception, we generated deletion mutants for *CCKLR-17D1* and *CCKLR-17D3* using CRISPR/Cas9 genome editing and tested them for thermal nociception (Fig. 1C-F). When stimulated with a 42 °C probe, three independent deletion lines of the *CCKLR-17D1* and *CCKLR-17D3* exhibited thermal hypersensitivity (Fig. 1D and F), further supporting the role of DSK signaling in

the negative regulation of thermal nociception. To examine whether the phenotypes of *CCKLR-17D1* and *CCKLR-17D3* mutants are classified as hyperalgesia (hypersensitivity to normally noxious stimuli) or allodynia (abnormal hypersensitivity to normally innocuous stimuli), we tested the receptor mutants with a 38 °C probe, which is close to the threshold of larval thermal nociception (39 °C)[24]. We found that the responses of the DSK receptor mutants were indistinguishable from the controls, indicating that the DSK receptor mutants are hypersensitive to suprathreshold thermal stimuli, thus hyperalgesic (Fig. S1).

Two groups of brain neurons expressing DSK are responsible for regulating nociception

Next, we attempted to identify DSK-expressing cells in the larval CNS that are responsible for regulating nociception. Unlike mammalian CCK, which is expressed in the CNS and gastrointestinal system, *Drosophila* DSK is expressed in the CNS but not in the gut[19, 47-50]. Previous immunohistochemical studies have reported putative DSK-expressing cells in the larval CNS[47, 49]. However, since the specificity of the DSK antibodies has not been validated with null mutants in the former studies, it has been a concern that the reported DSK-expressing cells could include non-DSK cells that express the other neuropeptides sharing the C-terminal RFa motif with DSK[51]. Consistent with this concern, we found that an antibody against crustacean FLRFa, an FMRFa-like neuropeptide with the C-terminal RFa motif, gives rise to a comparable staining pattern to that of the previously reported DSK antibodies, visualizing cells designated as insulin-producing cells (IPCs; referred to as SP3 in Nichols and Lim, (1996)[47]), MP1, SP1, SP2, Sv, SE2, Tv1-3, T2dm, and A8 in the larval CNS (Fig. 2A)[47, 49].

To identify bona fide DSK-expressing cells responsible for regulating nociception, we performed anti-

FLRFa staining in multiple *dsk* null alleles and found that the staining signals persist in all but two pairs of neurons, MP1 and Sv, in the mutant CNS (Fig. 2B-D and S2A-D), suggesting that these two pairs of neurons are the only neurons in the larval CNS that express DSK. The genomic rescue fragment that rescued the thermal hypersensitivity of *dsk* mutants (Fig. 1B) also restored the anti-FLRFa signals in MP1 and Sv in a *dsk* mutant background (Fig. 2E), suggesting that the *dsk* gene is responsible for the anti-FLRFa signals in these neurons as well as the thermal nociceptive responses of larvae. This expression pattern was further corroborated by the transgenic reporter line *DSK-GAL4* and the 2A-GAL4 knock-in reporter line *DSK-2A-GAL4*, both of which we found were expressed only in MP1 and Sv neurons among the anti-FLRFa-positive neurons (Fig. 2A, C, and F; Fig. S2B-F). We also found that anti-FLRFa, *DSK-GAL4*, and *DSK-2A-GAL4* do not visualize larval peripheral neurons including C4da nociceptors (Fig. 2A and F; Fig. S2G). Taken together, these results identified two sets of brain neurons, MP1 and Sv, as the DSK-expressing cells that are potentially involved in regulating nociception in larvae.

CCKLR-17D1 in Goro neurons functions to negatively regulate nociception

Next, we sought potential target cells of DSK signaling for regulating nociception. Since DSK receptor mutants were thermally hypersensitive consistently to *dsk* mutants (Fig. 1B, D, and F), neurons in the larval nociceptive circuit that express DSK receptors were promising candidates. To visualize the cells expressing DSK receptors, we generated T2A-GAL4 knock-ins in *CCKLR* genes. Both *CCKLR-17D1-T2A-GAL4* and *CCKLR-17D3-T2A-GAL4* were widely expressed in the larval CNS, predominantly in neuronal cells (Fig. 3A and B; Fig. S3A-D). By performing double-labeling experiments, we found that *CCKLR-17D1-T2A-GAL4* and *CCKLR-17D3-T2A-GAL4*

are not expressed in the nociceptors at the periphery (Fig. 3C and D; Fig. S3E and F), or in nociceptive interneurons including Basin1-4[52], A08n[36, 41], and DnB neurons[35] in the larval VNC (Fig. S3G-L). However, we found that they are expressed in Goro neurons (Fig. 3E and F), which are the fourth-order nociceptive interneurons located in the larval VNC[52].

To test whether the DSK receptors in Goro neurons are functionally important for regulating nociception, we performed RNAi and rescue experiments using *R69E06-GAL4* that marks Goro neurons[52]. RNAi knockdown of CCKLR-17D1, but not CCKLR-17D3, in *R69E06-GAL4* neurons induced thermal hypersensitivity (Fig. 4A and Fig. S4A). *R69E06-GAL4* is also expressed in multiple neurons in the larval brain other than Goro neurons in the VNC[52]. However, the thermal hypersensitivity was not observed when the expression of CCKLR-17D1 RNAi was excluded from Goro neurons by *tsh-GAL80*, pointing to the requirement of CCKLR-17D1 in Goro neurons (Fig. S4B-D). Consistent with these RNAi results, expressing wild-type CCKLR-17D1, but not CCKLR-17D3, with *R69E06-GAL4* rescued the hypersensitivity of the respective mutants (Fig. 4B and C). Furthermore, the morphology of Goro neurons was not affected by CCKLR-17D1 knockdown (Fig. S4E). Therefore, we conclude that CCKLR-17D1 functions in Goro neurons to negatively regulate thermal nociception, but the function of CCKLR-17D3 in nociceptive regulations resides elsewhere.

Activation of Goro neurons elicits nocifensive rolling in larvae[52]. Hence, if CCKLR-17D1 functions in Goro neurons to negatively regulate nociception, these neurons should be sensitized to noxious heat with the lack of CCKLR-17D1. We directly addressed this hypothesis by using a Ca^{2+} imaging technique we developed

previously[32, 35], whereby we monitored GCaMP6m signals in Goro neurons while applying thermal ramp stimuli to the larval body wall. Goro neurons in *CCKLR-17D1*$^{\Delta 1}$ mutants showed a significantly steeper GCaMP6m signal increase from 40 to 50 °C in comparison with the wild-type controls (Fig. 5A and B, Movie S1 and S2). Since the baseline fluorescence levels of GCaMP6m were not significantly different in the wild-type and *CCKLR-17D1*$^{\Delta 1}$ mutants (Fig. 5C), these data demonstrate that Goro neurons in *CCKLR-17D1*$^{\Delta 1}$ mutants are specifically sensitized to a noxious range of heat. Suppressing CCKLR-17D1 by RNAi in Goro neurons also induced significantly sensitized responses of Goro to noxious temperatures of 44–49 °C (Fig. 5D-F, Movie S3 and S4). In contrast, Goro neurons in *CCKLR-17D3*$^{\Delta 1}$ mutants exhibited GCaMP6m signals that were mildly elevated but largely parallel compared with that of the controls (Fig. S5, Movie S5 and S6), providing further evidence for the major functioning of CCKLR-17D3 in nociceptive regulation outside Goro neurons. Overall, these data demonstrate that CCKLR-17D1 functions to negatively regulate the activity of Goro neurons, thereby attenuating behavioral nociceptive responses.

MP1 neurons serve as descending nociceptive inhibitory neurons and as the closest source of DSK for Goro neurons

Neuropeptides mediate not only synaptic transmission as neurotransmitters but also distant neuronal communications through diffusions[53, 54]. If CCKLR-17D1 is involved in regulating the activity of Goro neurons, how can DSK be conveyed from the brain to the VNC? We noticed that some of the *DSK-GAL4* positive brain neurons sent descending neural processes to the VNC (Fig. 6A), which were all anti-FLRFa positive (Fig. 6B).

Furthermore, the anti-FLRFa signals in the descending projections were completely absent in the *dsk* mutants (Fig. 6C), suggesting that these descending projections likely originated from the DSK-expressing brain cells, namely MP1 and/or Sv. In analyzing *DSK-2A-GAL4*, we found that MP1 neurons in fact sent the descending projections to the VNC (Fig. 6D). To further understand the projection patterns of MP1 and Sv neurons in detail, we performed single-cell labeling using an FLP-out technique and revealed that MP1 neurons sent descending projections contralaterally to the VNC (Fig. 6E and S6A), while Sv neurons projected within the brain (Fig. S6B). In comparison with the longitudinal processes to the VNC, MP1 neural processes in the brain possessed few anti-FLRFa positive puncta, which represent DSK in these neurons (Fig. 6F). Furthermore, when the somatodendritic marker *UAS-Denmark* and the synaptic vesicle marker *UAS-syt::eGFP* were expressed in MP1 neurons[55], Denmark preferentially localized in the neural processes within the brain while syt::eGFP strongly accumulated in the processes descending to the VNC (Fig. 6G). Collectively, these data demonstrate that MP1 neurons project DSK-positive descending axons to the VNC from the brain.

Next, we examined whether MP1 descending neurons are involved in the negative regulation of nociception by artificially activating these neurons using *DSK-2A-GAL4* and *UAS-dTRPA1*. dTRPA1 is a cation channel gated by warm temperature (> 29 °C), which has been used as a tool to artificially activate neurons of interest in *Drosophila*[56]. When the larvae expressing dTRPA1 in C4da nociceptors with *ppk1.9-GAL4* were placed in a 35 °C chamber, dTRPA1-induced thermogenetic activation of C4da nociceptors caused nocifensive rolling responses within two seconds in the majority of animals (Fig. 6H). In contrast, when the larvae expressing dTRPA1

simultaneously in *ppk1.9-GAL4* and *DSK-2A-GAL4* were placed in a 35 °C chamber, the additional activation of *DSK-2A-GAL4* neurons to C4da nociceptors resulted in a markedly reduced percentage of larvae showing rolling responses within two seconds and significantly lengthened latencies (Fig. 6H). These data suggest that *DSK-2A-GAL4* neuron activation causes nociceptive inhibition. None of the animals expressing dTRPA1 with *DSK-2A-GAL4* alone showed rolling responses in 10 seconds (Fig. 6H). Although the expression of *DSK-2A-GAL4* was not completely specific to MP1 neurons, MP1 neurons were the only cells that were labeled by *DSK-2A-GAL4* with 100% reproducibility while the expression of *DSK-2A-GAL4* in IPCs and Sv neurons was minor and stochastic (Fig. 2F). Therefore, the observed nociceptive inhibition caused by activating *DSK-2A-GAL4* neurons is mostly attributable to the activation of MP1 neurons and supports their role in negatively regulating nociception.

To gain more insights on how DSK can be transmitted to Goro neurons, we further examined the anatomical relationship between MP1 axons and Goro neurons in the VNC. Performing double-labeling experiments, we found that MP1 axons with anti-FLRFa signals (representing DSK in MP1 axons) partially overlapped with Goro neurites in the thoracic segments of the larval VNC (Fig. 6I). GFP reconstitution was reproducibly detected between MP1 and Goro neurons using the CD4-GRASP (GFP Reconstitution Across Synaptic Partners) system[57, 58], thus confirming that MP1 axons and Goro neurons are indeed in close proximity (Fig. 6J). Since the CD4-GRASP is known to detect general cell-cell contacts[59, 60], we further investigated whether MP1 and Goro neurons are synaptically connected by using the nSyb-GRASP technique, which specifically enables synapse detection by localizing one of the split-GFP fragments in presynaptic sites[61]. However, no signals of

reconstituted GFP were detected between MP1 and Goro with nSyb-GRASP, although we found proximate localizations of nSyb-GFP_{1-10} in the MP1 axons with the Goro neurites expressing CD4::GFP_{11} (Fig. 6K). We also employed the *trans*-Tango system[62] as another tool to detect synaptic connectivity. However, when the *trans*-Tango ligand was expressed by *DSK-2A-GAL4*, synaptic connectivity between MP1 and Goro was not indicated since the postsynaptic activation of *trans*-Tango signals was not observed in Goro neurons, although some *trans*-Tango-positive neurons were observed around Goro neurons (Fig. S6C).

Overall, these results identified DSKergic MP1 descending neurons as an inhibitory system of nociception in larvae, and the descending axons of MP1 neurons as the closest source of DSK for Goro neurons.

Discussion

In this study, we have demonstrated that (1) DSK and its receptor CCKLR-17D1 and CCKLR-17D3 are involved in negatively regulating thermal nociception, (2) Two sets of brain neurons, MP1 and Sv, are DSK-expressing neurons in the larval nervous system, (3) One of the DSK receptors CCKLR-17D1 functions in Goro neurons to negatively regulate thermal nociception, (4) Thermogenetic activation of MP1 neurons inhibit larval nociception induced by the activation of C4da nociceptors, and (5) MP1 neurons in the brain project DSK-positive descending axons which contact with Goro neurons in the VNC. Based on these data, we propose that the DSK/CCKLR-17D1 system regulating the activity of the Goro neurons constitutes a descending inhibitory pathway of nociception from the brain to the VNC in larval *Drosophila* (Fig. 7). To our knowledge, our findings represent the first evidence of a

descending mechanism to modulate nociception from the brain in a non-mammalian species.

DSK signaling as a physiological modulator of nociception

DSK has been implicated in multiple physiological and developmental processes in *Drosophila*[19, 21-23]. Previous studies have shown that *dsk* and *CCKLR-17D1* mutants exhibit significant reductions of synaptic growth and excitability in larval neuromuscular junctions (NMJ) and larval locomotion under bright light[45, 63], suggesting the importance of the DSK/CCKLR-17D1 signaling pathway in the developmental processes of motoneurons. However, in this study, no major developmental defects were observed in Goro neurons with CCKLR-17D1 RNAi (Fig. S4E). Furthermore, the simultaneous thermogenetic activations of *DSK-2A-GAL4* neurons and C4da nociceptors inhibited larval nociception (Fig. 6H). Given the pronociceptive role of Goro neurons, their reduced synaptic or neuronal activity should cause nociceptive insensitivity or reduced Ca^{2+} responses, which is contradicting to our observation that CCKLR-17D1 knockdown in Goro produced the thermal hypersensitivity and exaggerated Ca^{2+} responses (Fig 4 and 5). Thus, these data consistently support a physiological role of DSK/CCKLR-17D1 signaling in modulating the activity of Goro neurons rather than a developmental role and also highlight the functional differences of the DSK/CCKLR-17D1 pathway between the NMJ and the nociceptive system in the CNS.

DSK in larval IPCs dispensable for nociceptive modulation

A previous study has reported the expression of DSK in a population of larval IPCs and its functions in responding to starving conditions[49]. However, we observed that anti-FLRFa signals in IPCs persisted in *dsk* null mutants and that anti-FLRFa signals in IPCs hardly overlap with either *DSK-GAL4* or *DSK-2A-GAL4* expressions (Fig. 2 and

S2). Although we used a different antibody from that in the study mentioned above, the number of IPCs visualized by anti-FLRFa was comparable to that of cells visualized by anti-DSK (Fig. S2)[49]. Regarding the functions of IPCs in nociception, Im et al. showed that silencing *dilp2-GAL4* positive IPCs has no significant effect on the baseline nociceptive responses[64]. Thus, the current and previous studies strongly suggest that DSK in IPCs is likely irrelevant for larval nociceptive regulation at least under normal conditions, although it is still possible for DSK to be expressed stochastically in a limited population of IPCs.

Multiple scenarios for the transmission of DSK from the brain to Goro neurons

Although our data suggest the existence of the DSKergic descending inhibitory system which regulates larval nociception, there are multiple possible scenarios for how DSK is transmitted from the brain to Goro neurons in the VNC: The first scenario is that MP1 descending neurons serve as the source of DSK to regulate Goro neurons, and this is currently the most parsimonious model based on our findings. Our nSyb-GRASP and *trans*-Tango experiments consistently showed negative results, indicating no synaptic connectivity between MP1 and Goro neurons (Fig. 6K and S6C). Thus, in this scenario, the interaction between DSK from MP1 neurons and Goro neurons may be mediated non-synaptically through volume transmission as noted in many neuropeptidergic systems[53, 54]. Many of the CCKLR-expressing neurons in the VNC are located far from the descending axons of MP1 (Figure 3 and 6). As it is unlikely that all these CCKLR-expressing neurons are synaptically connected to MP1 axons, neuronal communications through volume transmission can be fairly assumed for DSKergic systems in the larval VNC.

The second scenario is that not only MP1 neurons but also Sv neurons serve as the source of DSK for Goro neurons. Although Sv neurons innervate ascendingly in the brain lobe, and their axon termini localize far from the VNC (Fig. S6B), we cannot eliminate the possibility that DSK from Sv neurons acts on Goro neurons given that some neuropeptides can function with distances in millimeters[54]. The third and the least likely scenario is that only Sv neurons contribute to DSK secretion to regulate Goro neurons. For this scenario to be true, MP1 neurons would be required to mediate nociceptive inhibition through a DSK-independent mechanism. One potential candidate for this may be the neuropeptide allatostatin C, which is reportedly co-expressed in the larval MP1 neurons[50] and implicated in modulating nociception through the immune system in adult flies[43], although its function in larval nociception has been unclear. Further analyses of the functional connectivity between DSKergic neurons and Goro neurons using finer genetic/neuronal manipulations as well as the circuitry connectivity at electron microscopic resolution between MP1 neurons and Goro neurons are required to clarify the transmission mechanism of DSK from the brain to Goro neurons.

Multiple mechanisms of DSK signaling in regulating nociception

The data presented in this study also suggest that DSK signaling could regulate larval nociception through multiple pathways other than the DSK/CCKLR-17D1 system. For example, while *CCKLR-17D3* mutants exhibited as severe thermal hypersensitivity as *CCKLR-17D1* mutants (Fig. 1D and F), our RNAi and rescue experiments failed to locate the function of CCKLR-17D3 to Goro neurons (Fig. 4A and C). Our Ca^{2+} imaging also revealed that Goro neurons lacking CCKLR-17D3 showed modestly sensitized responses to noxious heat (Fig. S5). These results

suggest the major functioning of CCKLR-17D3 in Goro-independent nociceptive pathways. We also observed that DSK receptor mutants exhibited more severe thermal phenotypes than *dsk* mutants (Fig. 1). Although there has been no clue as to this difference between *dsk* and receptor mutants, it might indicate complex functions of DSK signaling pathways in regulating nociception. Further research is apparently necessary to reveal the whole picture of nociceptive regulations mediated by DSK and its receptors in larval *Drosophila*.

Potential conservation of CCK-mediated descending nociceptive controls

The CCK system is thought to be one of the most ancient neuropeptide systems, suggested to have multiple common physiological functions across taxa[16-20]. In this study, we demonstrate that CCKergic signaling in *Drosophila* participates in nociceptive modulation through a descending inhibitory pathway similarly to the mammalian CCK system, adding new evidence about the conserved physiological roles of CCK.

Unlike the peripheral nociceptive systems, it is still challenging to align the *Drosophila* and mammalian CCKergic descending pathways due to low homologies of the CNS structures between *Drosophila* and mammals, wide-spread CCK expression in the mammalian CNS, and the multiple roles of the CCKergic systems in mammalian nociceptive controls[10-14, 65-69]. However, the common usage of an orthologous molecular pathway in descending controls of nociception between the two evolutionarily distant clades raises a fascinating new hypothesis that the descending control from the brain may also be an ancient, conserved mechanism of nociception, which has emerged in the common ancestor of protostomes and deuterostomes. It will be of interest for future research to investigate whether the role of CCK signaling in descending nociceptive controls is also present in other species.

Potentials of non-mammalian models to study the mechanisms of pain modulation and pain pathology in the CNS

Non-mammalian model systems have been increasingly recognized as powerful tools to identify novel pain-related molecular pathways[2, 70-73]. However, the utilization of these models has so far been mostly limited to the research on peripheral pain pathophysiology, and few studies have used them to investigate central pain pathophysiology [2, 74]. Descending nociceptive control mechanisms are crucial for central pain modulation and have been implicated in the development of chronic pain states in humans[5, 6]. Thus, the current study opens the door to a new approach to using powerful neurogenetic tools and the simpler nervous system of *Drosophila* for elucidating the functional principles of descending nociceptive systems, which may potentially contribute to our understanding of the mechanisms underlying central pain modulation and pain pathology due to dysfunctions of descending modulatory pathways.

Acknowledgments

We thank the NIG-Fly Stock Center, TRiP at Harvard Medical School (NIH/NIGMS R01-GM084947), the Bloomington Stock Center, and Drs. Masayuki Koganezawa, Takeshi Awasaki, Barry Ganetzky, and Marta Zlatic for fly stocks. We are grateful to Dr. Eve Marder for kindly providing the anti-FLRFa antibody. We also thank Drs. Yoshiki Hayashi, Makoto Hayashi, and Satoru Kobayashi for their support in imaging with Leica SP5 and SP8, and Ms. Megumi Hamajima for technical assistance. This study was supported by grants from JSPS KAKENHI to K

Honjo (17K14928 and 19K06935) and HT (17H01378 and 26250001), and grants from the National Center for Geriatrics and Gerontology (21-47), the Uehara Memorial Foundation, and the Mochida Memorial Foundation for Medical and Pharmaceutical Research to K Honjo.

Author contributions: K Honjo conceived of the research. IO, K Hashimoto, AK, and K Honjo performed experiments and analyzed data. SK and HT generated *dsk*^{sk1} mutant and DSK receptor GAL4 lines. K Honjo wrote the manuscript with input and edits from IO, SK, HT, and KFT.

Declaration of interests: Authors declare no competing interests.

Figures and figure legends

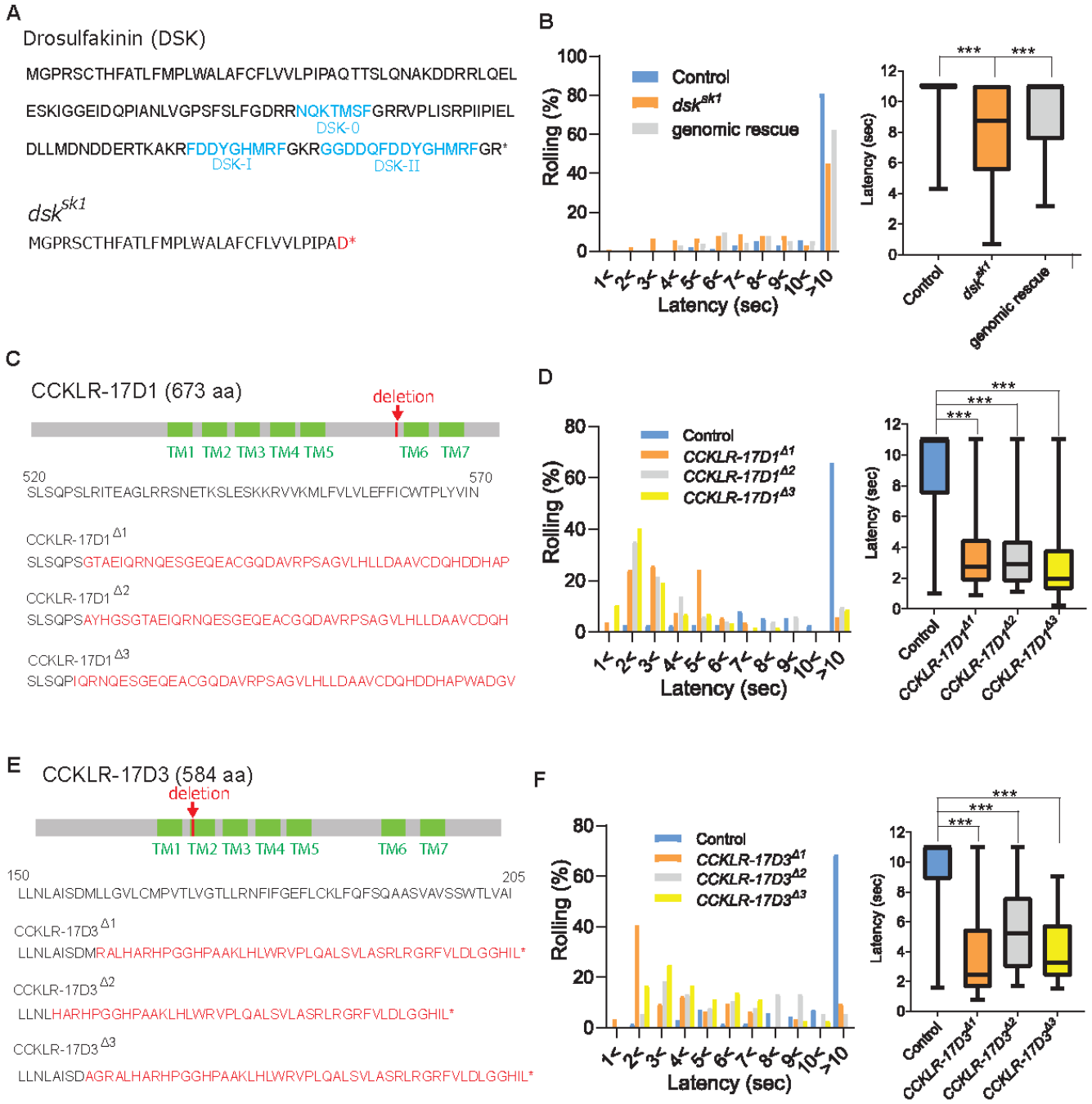

Fig 1. DSK signaling is involved in negatively regulating nociception.

(A) Predicted amino acid sequences of pro-DSK peptide in the wild-type (top) and *dsk*^{sk1} mutants (bottom). Due to

a 5-base deletion at the +94-99 position in the coding sequence, *dsk*^{sk1} mutants are predicted to produce a largely truncated pro-DSK peptide unable to be processed to active DSK peptides. Red letters represent residues different from the wild-type and asterisks indicate stop codons. (B) Hypersensitivity of *dsk*^{sk1} mutants to a 42°C thermal probe. Significantly shortened latencies of *dsk*^{sk1} mutants (n = 143) compared with the controls (n = 164) were recovered in genomic rescue animals (*Dp(3;1)2-2*; *dsk*^{sk1}, n = 139). (Left) Histograms (Right) Box plots of latencies. *** $p < 0.001$ Steel's test. (C) Predicted amino acid sequence of CCKLR-17D1 in the wild-type and *CCKLR-17D1* mutants. *CCKLR-17D1*$^{\Delta 1}$, *CCKLR-17D1*$^{\Delta 2}$, and *CCKLR-17D1*$^{\Delta 3}$ have 17-base (+1573-1589), 2-base (+1575-1576) and 32-base (+1573-1604) deletions in the coding sequence respectively, which result in large frameshifts completely abolishing the sixth and seventh transmembrane domains (TMs). (D) *CCKLR-17D1*$^{\Delta 1}$ (n = 54), *CCKLR-17D1*$^{\Delta 2}$ (n = 51) and *CCKLR-17D1*$^{\Delta 3}$ mutants (n = 57) all showed significantly shorter latencies than control (n = 38). (Left) Histograms (Right) Box plots of latencies. *** $p < 0.001$ Steel's test. (E) Predicted amino acid sequence of CCKLR-17D3 in the wild-type and *CCKLR-17D3* mutants. *CCKLR-17D3*$^{\Delta 1}$, *CCKLR-17D3*$^{\Delta 2}$, and *CCKLR-17D3*$^{\Delta 3}$ possess 8-base (+474-481), 32-base (+457-488), and 5-base (+472-476) deletions in the coding sequence respectively, which result in large frameshifts and truncation in the middle of the second TM. (F) *CCKLR-17D3*$^{\Delta 1}$ (n = 32), *CCKLR-17D3*$^{\Delta 2}$ (n = 38), and *CCKLR-17D3*$^{\Delta 3}$ mutants (n = 36) all exhibited significantly shorter latencies than control (n = 70). (Left) Histograms (Right) Box plots of latencies. *** $p < 0.001$ Steel's test. All box plots show median (middle line) and 25th to 75th percentiles with whiskers indicating the smallest to the largest data points.

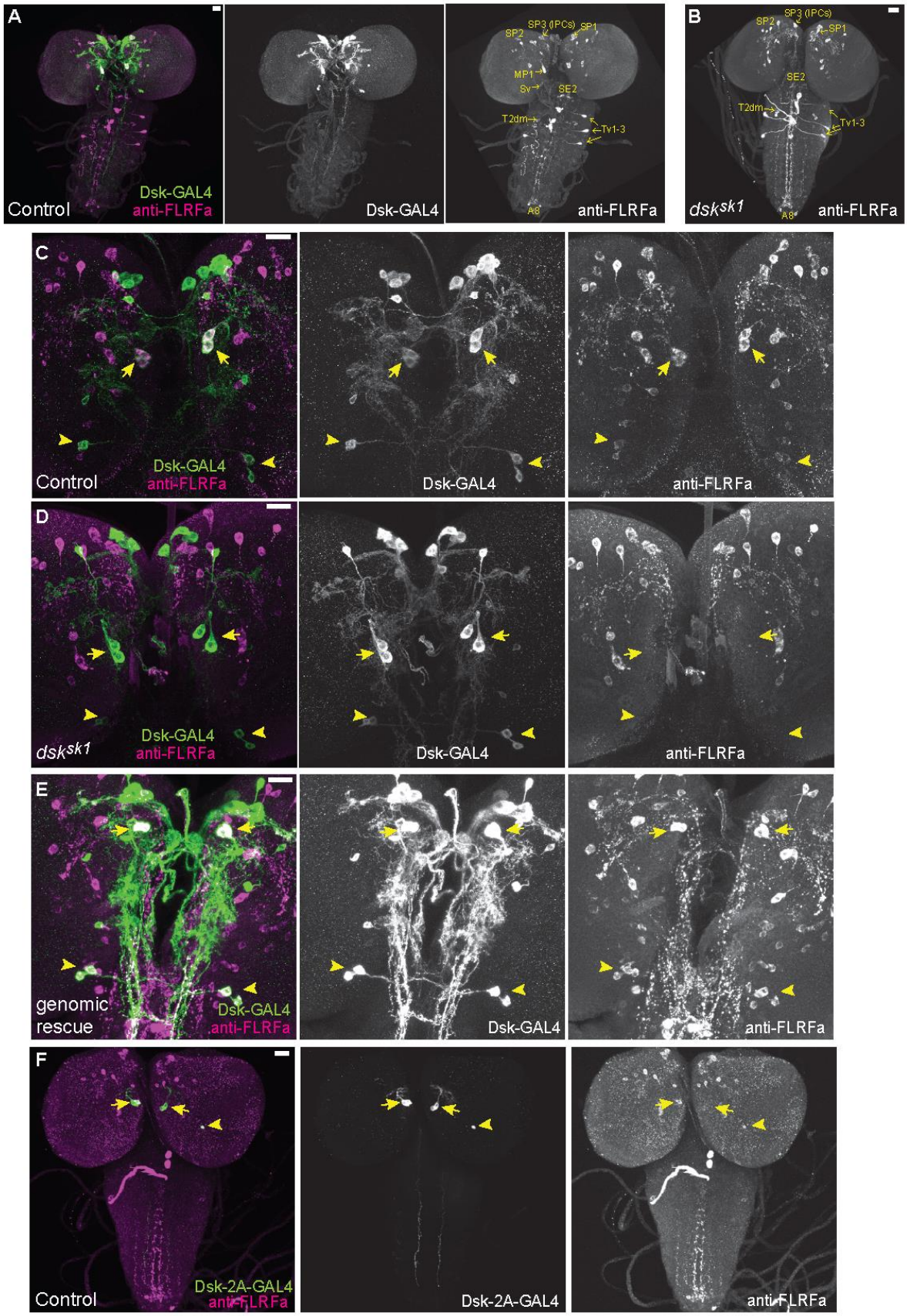
A
Control
Dsk-GAL4
anti-FLRFa
Dsk-GAL4
SP3 (IPCs)
SP2
SP1
MP1
Sv
SE2
T2dm
Tv1-3
A8
anti-FLRFa
B
SP3 (IPCs)
SP2
SP1
SE2
T2dm
Tv1-3
A8
dsksk1
anti-FLRFa
C
Control
Dsk-GAL4
anti-FLRFa
Dsk-GAL4
anti-FLRFa
D
dsksk1
Dsk-GAL4
anti-FLRFa
Dsk-GAL4
anti-FLRFa
E
genomic
rescue
Dsk-GAL4
anti-FLRFa
Dsk-GAL4
anti-FLRFa
F
Control
Dsk-2A-GAL4
anti-FLRFa
Dsk-2A-GAL4
anti-FLRFa

332

Fig 2. DSK is expressed in two groups of larval brain neurons.

(A) Representative image of *DSK-GAL4* expression and anti-FLRFa staining in the wild-type larval CNS. (B) Representative image of anti-FLRFa staining in *dsk*^{sk1} larval CNS. (C) Representative images of *DSK-GAL4* expression and anti-FLRFa staining in the control larval brains. Arrows and arrowheads indicate MP1 and Sv neurons, respectively. Co-expressions of DSK-GAL4 and anti-FLRFa were observed in MP1 and Sv in all of examined samples (n = 27/27), but in IPCs only in 7% (n = 2/27). (D) Representative images of *DSK-GAL4* expression and anti-FLRFa staining in the *dsk*^{sk1} larval brains. Arrows and arrowheads indicate MP1 and Sv neurons, respectively. (E) Representative images of *DSK-GAL4* expression and anti-FLRFa staining in the larval brains of the genomic rescue genotype (*Dp(3;1)2-2*/Y; +/*lexA-rCD2::RFP UAS-mCD8::GFP*; *dsk*^{sk1} *DSK-GAL4*/*dsk*^{sk1}). Arrows and arrowheads indicate MP1 and Sv neurons, respectively. (F) An example image showing the expression of *DSK-2A-GAL4*, a 2A-GAL4 knock-in line of the *dsk* gene, more faithfully recapitulating its endogenous expression. Arrows and arrowheads indicate MP1 and Sv neurons, respectively. MP1 neurons were labeled in 100% of *DSK-2AGAL4* samples (n = 41/41), while a single IPC in 51.2% (n = 21/41), multiple IPCs in 24.4% (n = 10/41), and Sv neurons in 17.1% (n = 7/41) of examined samples. All scale bars represent 20 μm.

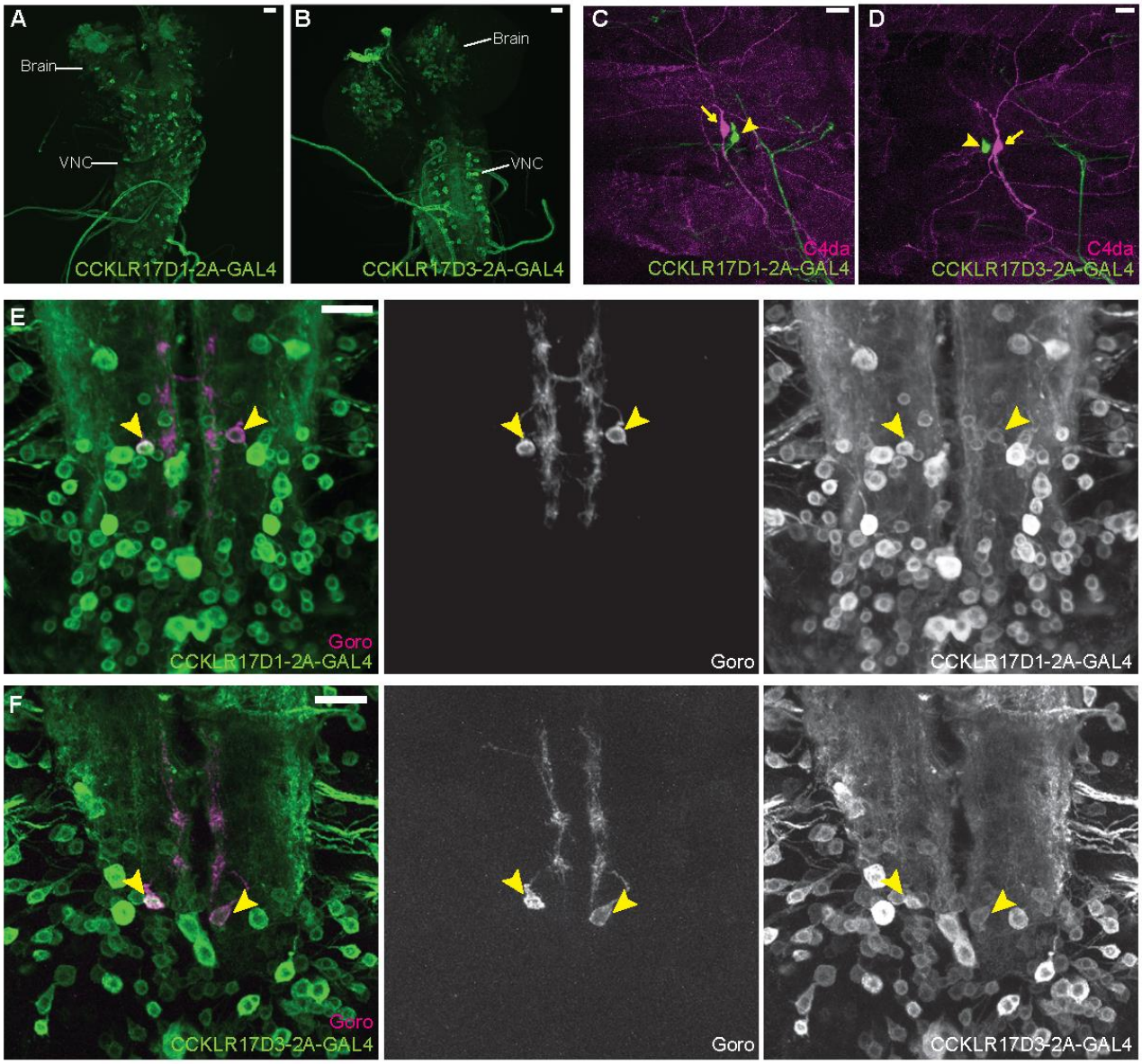

Fig 3. DSK receptors are expressed in Goro neurons in the larval VNC.

(A and B) Representative images of *CCKLR-17D1-T2A-GAL4* (A) and *CCKLR-17D3-T2A-GAL4* (B) expressions in the larval CNS. (C and D) Representative images showing double-labeling of *CCKLR-17D1-T2A-GAL4* (C) and *CCKLR-17D3-T2A-GAL4* (D) with C4da nociceptors (*R38A10-lexA*). Arrows and arrowheads indicate cell bodies of C4da nociceptors and es cells, respectively. (E and F) Representative images showing double-labeling of *CCKLR-*

17D1-T2A-GAL4 (E) and *CCKLR-17D3-T2A-GAL4* (F) with Goro neurons (arrowheads, *R69E06-lexA*). Expression patterns were confirmed in multiple samples (n = 7 and 5). All scale bars represent 20 µm.

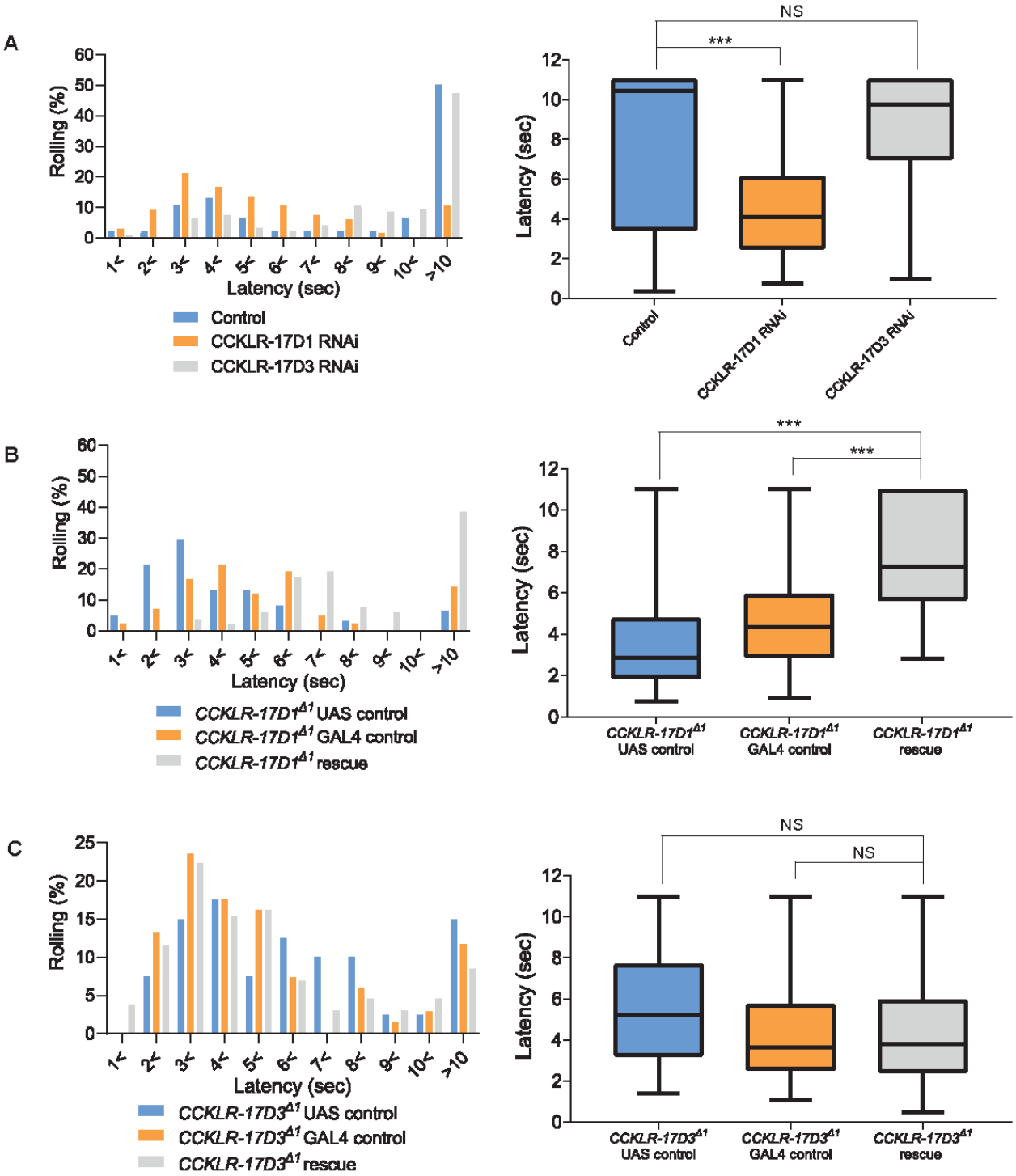

Fig 4. CCKLR-17D1 in Goro neurons is necessary and sufficient for normal thermal nociception.

(A) RNAi of CCKLR-17D1 and CCKLR-17D3 using a Goro-GAL4 line *R69E06-GAL4*. Expressing CCKLR-17D1 RNAi (*R69E06-GAL4* x *yv; JF02644*, n = 66) but not CCKLR-17D3 RNAi (*R69E06-GAL4* x *yv; JF02968*, n = 95) with *R69E06-GAL4* caused significantly shorter latencies to 42 °C than controls (*R69E06-GAL4* x *yv; attp2*, n = 46). (Left) Histograms (Right) Box plots of latencies. *** $p < 0.001$, NS (non-significant) $p > 0.05$ Steel's test. (B) Rescue of CCKLR-17D1 with *R69E06-GAL4*. The shortened latencies of *CCKLR-17D1*$^{\Delta 1}$ mutants observed in UAS controls (*CCKLR-17D1*$^{\Delta 1}$; *UAS-CCKLR-17D1/+*, n = 61) or GAL4 controls (*CCKLR-17D1*$^{\Delta 1}$; *R69E06-GAL4/+*, n = 42) were restored in the rescue genotype (*CCKLR-17D1*$^{\Delta 1}$; *UAS-CCKLR-17D1/+; R69E06-GAL4/+*, n = 52). (Left) Histograms (Right) Box plots of latencies. *** $p < 0.001$ Steel's test. (C) Rescue of CCKLR-17D3 with *R69E06-GAL4*. The shortened latencies of *CCKLR-17D3*$^{\Delta 1}$ mutants were unaltered in the rescue genotype (*CCKLR-17D3*$^{\Delta 1}$; *UAS-CCKLR-17D3/+; R69E06-GAL4/+*, n = 130) compared with UAS controls (*CCKLR-17D3*$^{\Delta 1}$; *UAS-CCKLR-17D3/+*, n = 40) or GAL4 controls (*CCKLR-17D3*$^{\Delta 1}$; *R69E06-GAL4/+*, n = 68). (Left) Histograms (Right) Box plots of latencies. NS (non-significant) $p > 0.05$ Steel's test. All box plots show median (middle line) and 25th to 75th percentiles with whiskers indicating the smallest to the largest data points.

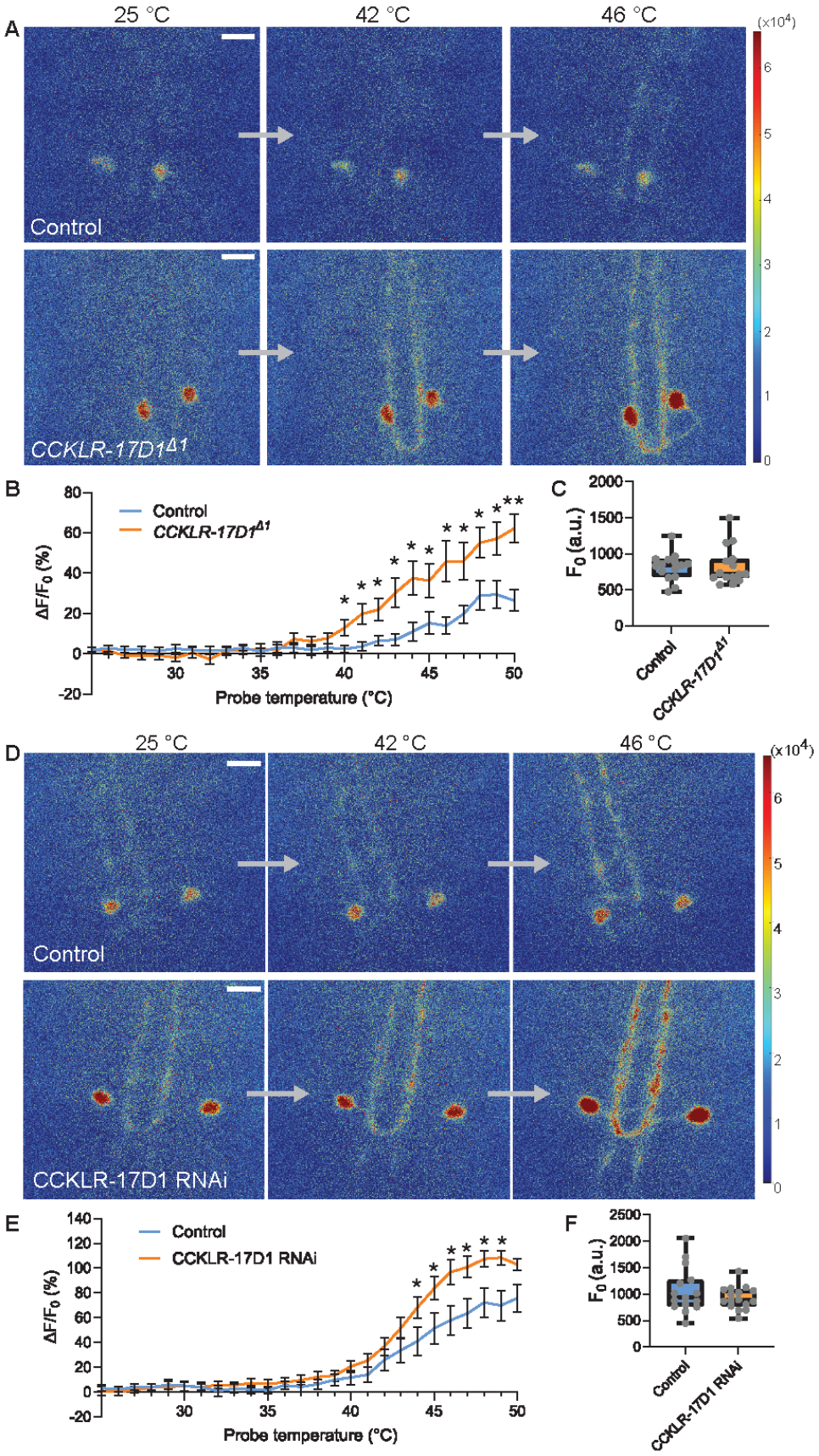
A
25 °C
42 °C
46 °C
(x10⁴)
Control
CCKLR-17D1Δ1
B
Control
CCKLR-17D1Δ1
ΔF/F0 (%)
Probe temperature (°C)
C
F0 (a.u.)
Control
CCKLR-17D1Δ1
D
25 °C
42 °C
46 °C
(x10⁴)
Control
CCKLR-17D1 RNAi
E
Control
CCKLR-17D1 RNAi
ΔF/F0 (%)
Probe temperature (°C)
F
F0 (a.u.)
Control
CCKLR-17D1 RNAi

370

Fig 5. Goro neurons lacking CCKLR-17D1 show sensitized responses to noxious heat.

(A) Representative still images showing thermal activation of Goro neurons in the controls (top, *yw*/Y; *R69E06-GAL4 UAS-GCaMP6m*/+) and *CCKLR-17D1*$^{\Delta 1}$ mutants (bottom, *CCKLR-17D1*$^{\Delta 1}$*/Y; R69E06-GAL4 UAS-GCaMP6m*/+). See also Movie S1 and S2. (B) Average percent increase of GCaMP6m fluorescence intensity relative to the baseline ($\Delta F/F_0$) during heat ramp stimulations in controls (n = 15) and *CCKLR-17D1*$^{\Delta 1}$ (n = 15). * $p < 0.05$, ** $p < 0.01$ Mann-Whitney's U-test. Scale bars represent standard error. (C) Basal GCaMP6m signal levels (F_0) in controls (n = 15) and *CCKLR-17D1*$^{\Delta 1}$ mutants (n = 15). $p > 0.6$ Mann-Whitney's U-test. (D) Representative stills showing thermal activation of the controls (top, *R69E06-GAL4 UAS-GCaMP6m* x *yv; attp2*) and Goro neurons expressing CCKLR-17D1 RNAi (bottom, *R69E06-GAL4 UAS-GCaMP6m* x *yv; JF02644*). See also Movie S3 and S4. (E) Average percent increase of GCaMP6m fluorescence intensity relative to the baseline ($\Delta F/F_0$) during heat ramp stimulations in controls (n = 15) and CCKLR-17D1 RNAi (n = 16). * $p < 0.05$ Mann-Whitney's U-test. Scale bars represent standard error. (F) Basal GCaMP6m levels (F_0) in controls (n = 15) and CCKLR-17D1 RNAi (n = 16). $p > 0.6$ Mann–Whitney's U-test. All box plots show median (middle line) and 25th to 75th percentiles with whiskers indicating the smallest to the largest data points. All scale bars represent 20 µm.

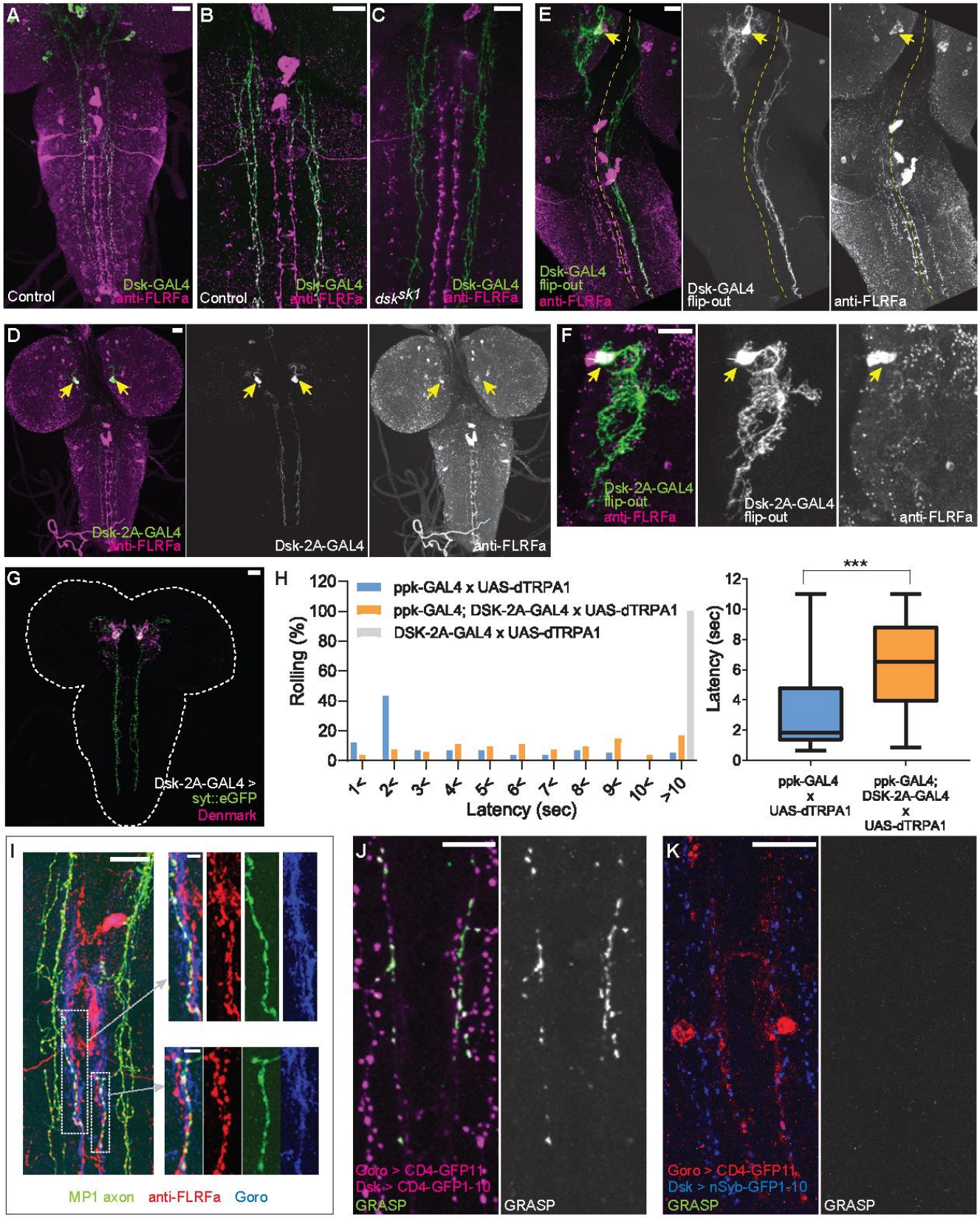
A
Control
Dsk-GAL4
anti-FLRFa
B
Control
Dsk-GAL4
anti-FLRFa
C
dsksk1
Dsk-GAL4
anti-FLRFa
E
Dsk-GAL4
flip-out
anti-FLRFa
Dsk-GAL4
flip-out
anti-FLRFa
D
Dsk-2A-GAL4
anti-FLRFa
Dsk-2A-GAL4
anti-FLRFa
F
Dsk-2A-GAL4
flip-out
anti-FLRFa
Dsk-2A-GAL4
flip-out
anti-FLRFa
G
Dsk-2A-GAL4 >
syt::eGFP
Denmark
H
ppk-GAL4 x UAS-dTRPA1
ppk-GAL4; DSK-2A-GAL4 x UAS-dTRPA1
DSK-2A-GAL4 x UAS-dTRPA1
Rolling (%)
Latency (sec)
1< 2< 3< 4< 5< 6< 7< 8< 9< 10< >10
***
Latency (sec)
ppk-GAL4 x UAS-dTRPA1
ppk-GAL4; DSK-2A-GAL4 x UAS-dTRPA1
I
MP1 axon
anti-FLRFa
Goro
J
Goro > CD4-GFP11
Dsk > CD4-GFP1-10
GRASP
GRASP
K
Goro > CD4-GFP11
Dsk > nSyb-GFP1-10
GRASP
GRASP

385

Fig 6. DSK-expressing MP1 neurons are descending neurons that inhibit nociception.

(A) Representative image showing descending axons from *DSK-GAL4* positive brain neurons (green) to the larval VNC. (B) Representative image showing all descending projections labeled by *DSK-GAL4* (green) harbor punctate anti-FLRFa signals (magenta) in the wild-type. (C) Representative image showing the complete absence of punctate anti-FLRFa signals (magenta) in the descending projections labeled by *DSK-GAL4* (green) in the dsk^{sk1} mutants. (D) Image showing the descending projections of MP1 neurons (arrows) marked by *DSK-2A-GAL4*. (E) Image showing a single FLP-out clone of MP1 neuron (arrow) contralaterally sending descending axons to the larval VNC. The yellow dashed line indicates the midline. (F) A projection image showing the MP1 neurites in the brain. Note that few anti-FLRFa-positve puncta are associated with MP1 neurites within the brain. Similar expression patterns were observed in multiple samples (n = 3). The arrow indicates the anti-FLRFa-positve MP1 soma. (G) Representative image showing localizations of syt::eGFP (green) and Denmark (magenta) in MP1 neurons (*DSK-2A-GAL4* x *UAS-syt::eGFP UAS-Denmark*). Similar expression patterns were observed in multiple samples (n = 7) (H) Thermogenetic activations of nociceptors and/or *DSK-2A-GAL4* neurons using *UAS-dTRPA1*. (Left) Histograms. Upon thermogenetic activations, 55% of larvae expressing dTRPA1 in nociceptors *(ppk1.9-GAL4* x *UAS-dTRPA1*, n = 58) exhibited nociceptive rolling in 2 seconds. In contrast, only 11% of larvae with simultaneous activations of nociceptors and *DSK-2A-GAL4* showed rolling in in 2 seconds (*ppk1.9-GAL4 DSK-2A-GAL4* x *UAS-dTRPA1*, n = 54). Thermogenetic activations of *DSK-2A-GAL4* neurons alone (*DSK-2A-GAL4* x *UAS-dTRPA1*, n = 40) did not trigger nociceptive responses even after 10 seconds. (Right) Box plots of latencies showing median

(middle line) and 25th to 75th percentiles with whiskers indicating the smallest to the largest data points. Thermogenetic activations of *DSK-2A-GAL4* simultaneously with nociceptors caused a significantly longer latency to rolling responses (Mann-Whitney U-test, $p < 0.001$). (I) Representative images of the larval VNC showing partially overlapping MP1 axons (green) and processes of Goro neurons (blue) that are associated with anti-FLRFa signals (red). MP1 axons partially overlapping Goro neurons were similarly observed in all examined samples (n = 5). (J) Representative image showing CD4-GRASP experiments between MP1 axons and Goro neurons (Magenta). Signals of reconstituted GFP (GRASP, green) were detected in all examined samples (n = 5). (K) Representative image showing nSyb-GRASP experiments between MP1 axons (blue) and Goro neurons (red). Signals of reconstituted GFP (GRASP, green) were not detectable in any examined samples (n = 5). All scale bars represent 20 µm, except for in the insets of (I) (5 µm).

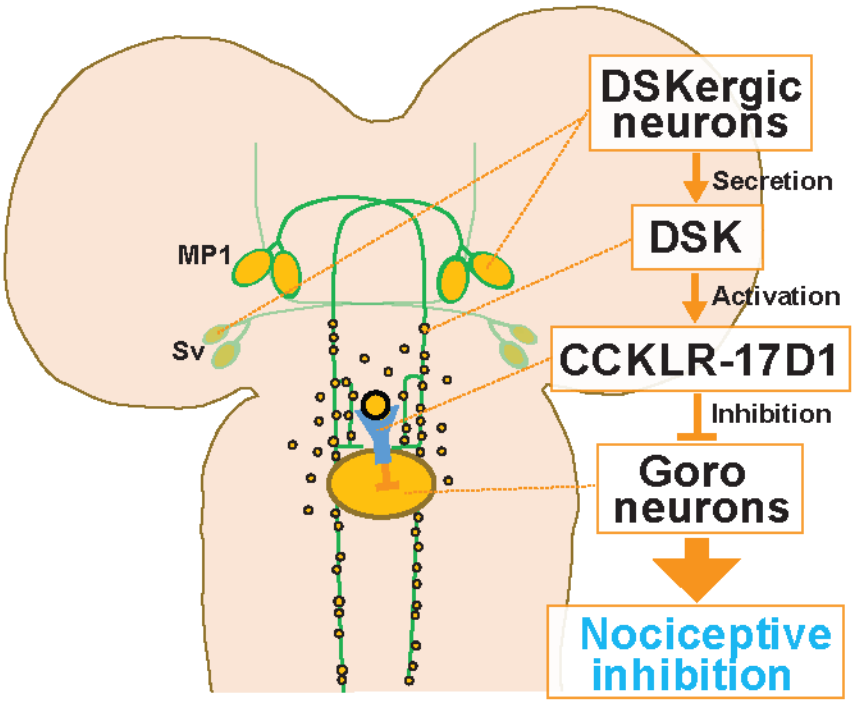

Fig 7. A schematic model of the DSKergic descending inhibitory pathway of nociception in larval *Drosophila*. DSK-expressing MP1 and Sv neurons in the brain secret DSK peptides. DSK in the larval VNC activates the CCKLR-17D1 receptor expressed in Goro neurons, which subsequently inhibits the activity of Goro neurons, and ultimately larval nociceptive rolling responses.

Materials and Methods

Fly strains

y^1w^{1118} strain was used as the control strain for *dsk*, *CCKLR-17D1*, and *CCKLR-17D3* mutants. *yv*; attp2 strain was used for the control of *yv; JF02644* (CCKLR-17D1 RNAi) and *yv; JF02968* (CCKLR-17D3 RNAi). *yw; nos-Cas9/CyO* (NIG-FLY CAS-0011) and *yw; Pr Dr/TM6C Sb Tb* were used for CRISPR/Cas9 mutagenesis. *Dp(3;1)2-2, w^{1118}; Df(3R)2-2/TM3 Sb* (Bloomington #3688), *UAS-CCKLR-17D1* [63], and *UAS-CCKLR-17D3* (this study) were used for rescue experiments. *DSK-GAL4* (Bloomington #51981), *DSK-2A-GAL4* (Bloomington #84630), *R69E06-GAL4* (Bloomington #39493), *R69E06-lexA* (Bloomington #54925), *R72F11-lexA* [52], *R70F01-lexA* (Bloomington #53628), *R38A10-lexA* (Bloomington #54106), *R82A10-lexA* (Bloomington #54417), *CCKLR-17D1-T2A-GAL4* [75], *CCKLR-17D3-T2A-GAL4* [75] and *tsh-GAL80* were used for tissue-specific gene expressions. *40xUAS-IVS-mCD8::GFP* (Bloomington #32195), *10xUAS-IVS-mCD8GFP* (Bloomington #32186), *UAS>CD2 stop>mCD8::GFP hs-flp* [76], *lexA-rCD2::RFP UAS-mCD8::GFP* [77], *ppk-CD4::tdGFP* (Bloomington #35842), *UAS-nSyb-GFP_{1-10}; lexAop-CD4-GFP_{11}* (Bloomington #64314), *UAS-CD4-GFP_{1-10}; lexAop-CD4-GFP_{11}* (Bloomington #58755), *UAS-Denmark UAS-syt::eGFP* (Bloomington #33065), and *UAS-myrGFP QUAS-mtdTomato::3xHA; trans-Tango* (Bloomington #77124) were used for cellular visualizations. *UAS-GCaMP6m* (Bloomington #42748) was used for Ca^{2+} imaging. *UAS-dTRPA1* (Bloomington #26263)[56] was used for thermogenetic experiments. *dsk^{sk1}*, *CCKLR-17D1* deletion mutants, *CCKLR-17D3* deletion mutants, and *UAS-CCKLR-17D3* were generated in this study and described below. *dsk^{attp}* strain [78] was obtained from the Bloomington

stock center (#84497). Stocks were kept at 25°C with 12:12 hour light cycle on a standard food.

Generating mutants and transgenic lines

Deletion mutants of *dsk*, *CCKLR-17D1*, and *CCKLR-17D3* were generated as described previously [79]. Briefly, 23 bp-guide RNA (gRNA) sequences specific to the aimed region of the targeted genes were identified using an online tool (http://www.flyrnai.org/crispr/) and 20-bp sequences excluding PAM were cloned to the pBFv-U6.2 vector. Injections of the gRNA-pBFv-U6.2 vectors to yield transgenic fly strains were performed by BestGene Inc. The gRNA-expressing lines were crossed with a nos-Cas9 strain and about 20 independent F1 generations that could potentially possess modifications in the targeted genomic region were established. Lines that had a frameshifting deletion in the targeted region were screened through standard PCR and sequencing. The following gRNA and PCR primer sequences were used to generate *dsk*, *CCKLR-17D1*, and *CCKLR-17D3* mutants:

- *dsk*: GTAGACTAGTCGTCTGCGCT (gRNA), CCTCTAAACACTTGACAGCCGCGGTAACGG (forward primer), and CCGAAACGCATGTGACCGTAGTCATCG (reverse primer).
- *CCKLR-17D1*: GCTTCCGTGATACGCAGACTGGG (gRNA), ATGTGTTTTGTGGATACCCTGT (forward primer), and GGGCTATACCTCCA-TCAGTTTC (reverse primer).
- *CCKLR-17D3*: GCCATATCGGACATGCTGCTGGG (gRNA), GATAGGGA-TGGCTATATGGACACCGAGC (forward primer), and CTTAGCTGTCCCAATTCCCCCATCTTCT (reverse primer).

The UAS-CCKLR-17D3 line was generated through a ΦC31 integrase–based method. The oligo DNA

corresponding to the sequence of CCKLR-17D3 mRNA (+447-2201 of AY231149) was synthesized (Eurofins Genomics) and cloned into the pUASg.attB vector [80] using the pENTR/D-TOPO Gateway cloning kit (Thermo Fisher Scientific, MA). The sequence-verified UAS-CCKLR-17D3 construct was integrated into the attP40 site to yield transgenic lines. The injections were performed by BestGene Inc.

Thermal nociception assay

The experimenters were blinded to genotypes. Larval thermal nociception assays were performed as described previously [31] with slight modifications. A custom-made probe with a thermal feedback system was used. Unless otherwise noted, a thermal probe heated to 42 °C was used to detect hypersensitive phenotypes[32].

Thermogenetic activation experiments

The experimenters were blinded to genotypes. A 60 mm dish containing approximately 1 ml distilled water (testing chamber) was placed on a temperature-controlled plate MATS-SPE (TOKAI HIT, Shizuoka, Japan) set at 44.5 °C to equilibrate the water temperature in a testing chamber to 35 ± 1 °C, which was continuously monitored using a T-type thermocouple wire IT-23 (Physitemp, NJ), USB-TC01 (National Instruments), and the NI Signal Express software (National Instruments, TX). Wandering third instar larvae expressing dTRPA1 by *ppk1.9-GAL4* and/or *DSK-2A-GAL4* were harvested to another 60 mm dish at room temperature (23-25 °C), and gently transferred to the 35 °C testing chamber using a paintbrush. All experiments were performed and recorded under a binocular microscope with a camcorder, and the latency from the placement of larvae to rolling was measured offline for each larva.

Immunohistochemistry

The following antibodies were used in this study: chicken anti-GFP (Abcam, 1:500), mouse anti-GRASP (Sigma #G6539, 1:100) [61], mouse anti-rat CD2 (Bio-Rad, 1:200), rat anti-mCD8 (Caltag, 1:100), rabbit anti-FLRFa (a gift from Dr. Eve Marder, 1:5000) [81], rabbit anti-CD4 (Novus Biologicals, 1:500), mouse anti-REPO (Developmental Studies Hybridoma Bank 8D12, 1:5), rabbit anti-DsRed (Clontech #632496, 1:200), rat anti-HA (Roche 3F10, 1:100), goat anti-HRP-Cy3 (Jackson ImmunoResearch, 1:100), goat anti-rat Alexa488 (Invitrogen, 1:500), goat anti-chicken Alexa488 (Invitrogen, 1:500), goat anti-mouse Alexa546 (Invitrogen, 1:500), goat anti-rabbit Alexa546 (Invitrogen, 1:500), goat anti-rat Alexa633 (Invitrogen, 1:500), and goat anti-rabbit Alexa633 (Invitrogen, 1:500). Dissected larval tissues were fixed in 4% paraformaldehyde for 30 minutes and then stained as previously described [32]. The images were acquired by using a Zeiss LSM 510 with a 20x/0.75 Plan-Apochromat objective or 40x/1.0 Plan-Apochromat oil immersion objective, Zeiss LSM 700 with a 20x/0.75 Plan-Apochromat objective or 40x/1.0 Plan-Apochromat oil immersion objective, or Leica SP5 with a 40x/0.85 PL APO objective, and digitally processed using Zeiss LSM Image Browser, Leica LAS X Lite, and Adobe Photoshop.

GRASP and *trans*-Tango experiments

The CD4-GRASP experiments were performed by crossing the *R69E06-lexA DSK-GAL4* strain with the *UAS-CD4-GFP$_{1-10}$; lexAop-CD4-GFP$_{11}$*. The nSyb-GRASP experiments were performed by crossing the *R69E06-lexA DSK-GAL4* with the *UAS-nSyb-GFP$_{1-10}$; lexAop-CD4-GFP$_{11}$*. Wandering 3rd instar larvae were dissected and immunostained as mentioned above. The signals of the reconstituted GFP were detected using a GFP antibody

without cross-reaction to split-GFP fragments (Sigma #G6539)[61].

The *trans*-Tango experiments were performed by crossing the *R69E06-lexA, lexAop-rCD2::RFP UAS-mCD8::GFP; DSK-2A-GAL4* with *UAS-myrGFP QUAS-mtdTomato::3xHA; trans-Tango*. Wandering 3rd instar larvae were dissected and immunostained as mentioned above. The following combinations of the primary and secondary antibodies were used to avoid cross-contamination of fluorescent signals in microscopy: chick anti-GFP and anti-chick Alexa488, mouse anti-rCD2 and anti-mouse Alexa546, and rat anti-HA and anti-rat Alexa633.

FLP-out clone analysis

The *UAS>CD2 stop>mCD8::GFP hs-flp* strain was crossed with *DSK-GAL4* or *DSK-2A-GAL4* to seed vials. Heat-shock induction of FLP-out clones and immunostaining were performed as described previously [32]. The images of brain samples were acquired and digitally processed as described above.

Calcium imaging

Ca^{2+} imaging of Goro neurons was performed as described previously [32] with some modifications. Wandering third instar larvae expressing GCaMP6m [82] in Goro neurons by *R69E06-GAL4* were dissected in ice-cold hemolymph-like saline 3.1 (HL3.1) [83] and imaged in a custom-made imaging chamber containing the HL3.1 equilibrated to the room temperature (23-25 °C). A Leica SP8 confocal microscope with resonant scanning system was used to perform three-dimensional time-lapse imaging. Z-stacks consisting of 4 to 6 optical slices of 512 x 512 pixel images were acquired at approximately 0.5 to 1 Hz using a 10x/0.4 PL APO objective lens with a zoom factor of 8.0. During imaging, a local heat ramp stimulation was applied to the lateral side of the A5 to A7 segment with a custom-made

thermal probe. The probe temperature was controlled using a Variac transformer set at 20 V, which generated an approximately 0.6 °C/sec heat ramp stimulus. A T-type thermocouple wire was placed inside of the thermal probe to acquire the probe temperature readings and the data were acquired at 4 Hz through a digitizer USB-TC01 (National Instruments) and the NI Signal Express software (National Instruments). To minimize potential biases caused by day-to-day variations in imaging conditions and achieve fair comparisons, similar numbers of control and experimental genotypes were imaged side-by-side on the same day, using identical microscope settings.

Maximum intensity projections were generated from the time-series Z-stacks on Leica LAS X Lite and the subsequent analyses of the images and temperature log data were performed using a custom-made code in MATLAB (MathWorks, MA). The region of interest (ROI) was selected as a circular area with a diameter of 15 pixels that covered the neurites of Goro neurons. Cell bodies were not used for the quantification because of small and variable increases in GCaMP6m signals upon heat stimulation. Average fluorescent intensity (F) was calculated for the ROI for each time point. The average of Fs from the first five frames was used as the baseline fluorescent intensity (F_0) and percent changes of fluorescent intensity from the baseline [$\Delta F/F_0 = (F - F_0)/F_0$] was calculated for each time point. At least three ROIs were selected from areas that were expected to yield high GCaMP6m signal increases and the ROI that led to the highest peak $\Delta F/F_0$ was chosen for the subsequent statistical analysis. Samples whose highest peak $\Delta F/F_0$ was less than 10% were excluded from the analysis to avoid the potential skew of data by including dead/unhealthy samples. Because the images and probe temperatures could not be acquired at the same time, probe temperature for each time point was calculated by linear interpolation from the raw readings. For

comparisons among strains, $\Delta F/F_0$ data were binned and averaged in 1 °C intervals.

Data collection and statistical analyses

Mann–Whitney's U-test was used for pair-wise comparisons and Steel's test (the non-parametric equivalent of Dunnet's test) or Steel–Dwass test (the non-parametric equivalent of Tukey-Kramer test) were used for multiple comparisons. Statistical analyses were performed in KyPlot 5.0 and GraphPad Prism 9. The numbers of samples (n) for all experiments indicate the numbers of biological replicates. Each experiment was repeated at least twice on different days to check the reproducibility and all data were pooled for statistical analyses unless otherwise noted.

Supplemental information

Supplemental figures S1-S6

Supplemental Movies S1-S6

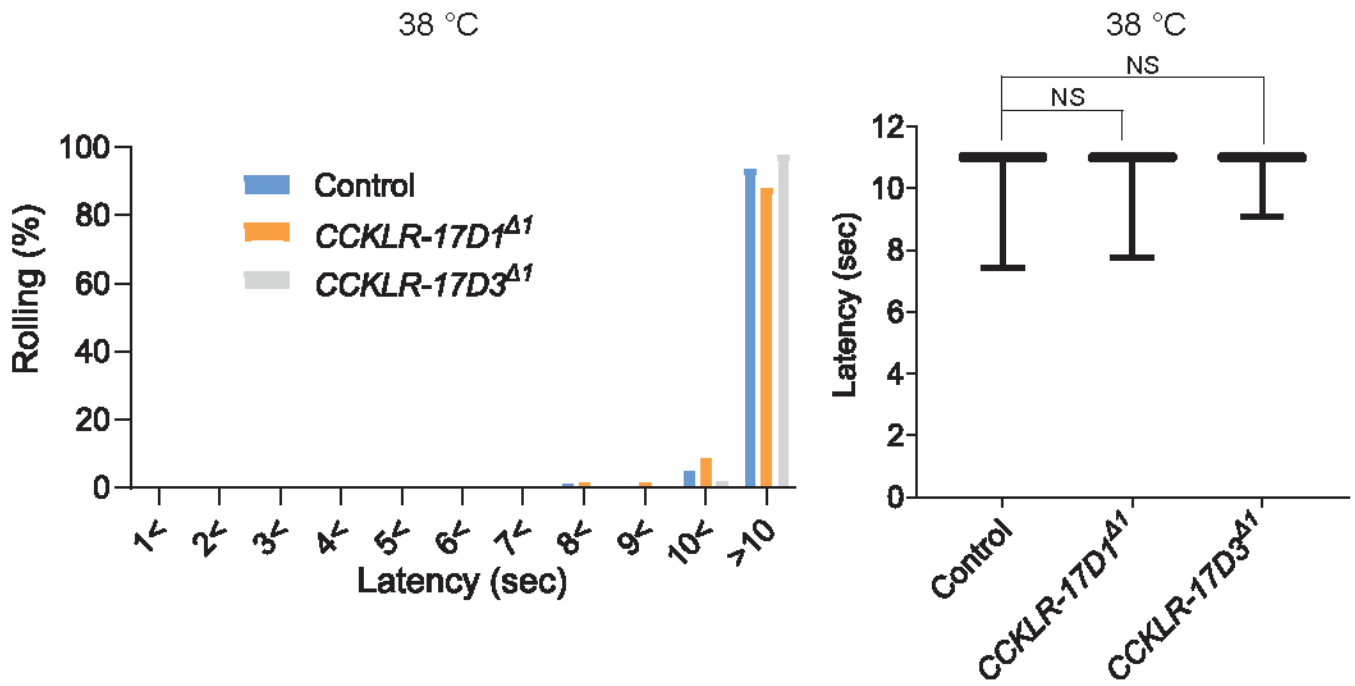

Fig. S1. Thermal nociceptive thresholds in DSK receptor mutants are largely normal (related to Fig. 1)

Thermal responses of *CCKLR-17D1* and *CCKLR-17D3* mutants to a 38 °C probe. Both *CCKLR-17D1*$^{\Delta 1}$ (n = 58) and *CCKLR-17D3*$^{\Delta 1}$ (n = 48) showed comparable distributions of responding latencies to the controls (*yw*, n = 79). Box plots show median (middle line) and 25th to 75th percentiles with whiskers indicating the smallest to the largest data points. $p > 0.4$ Steel's test.

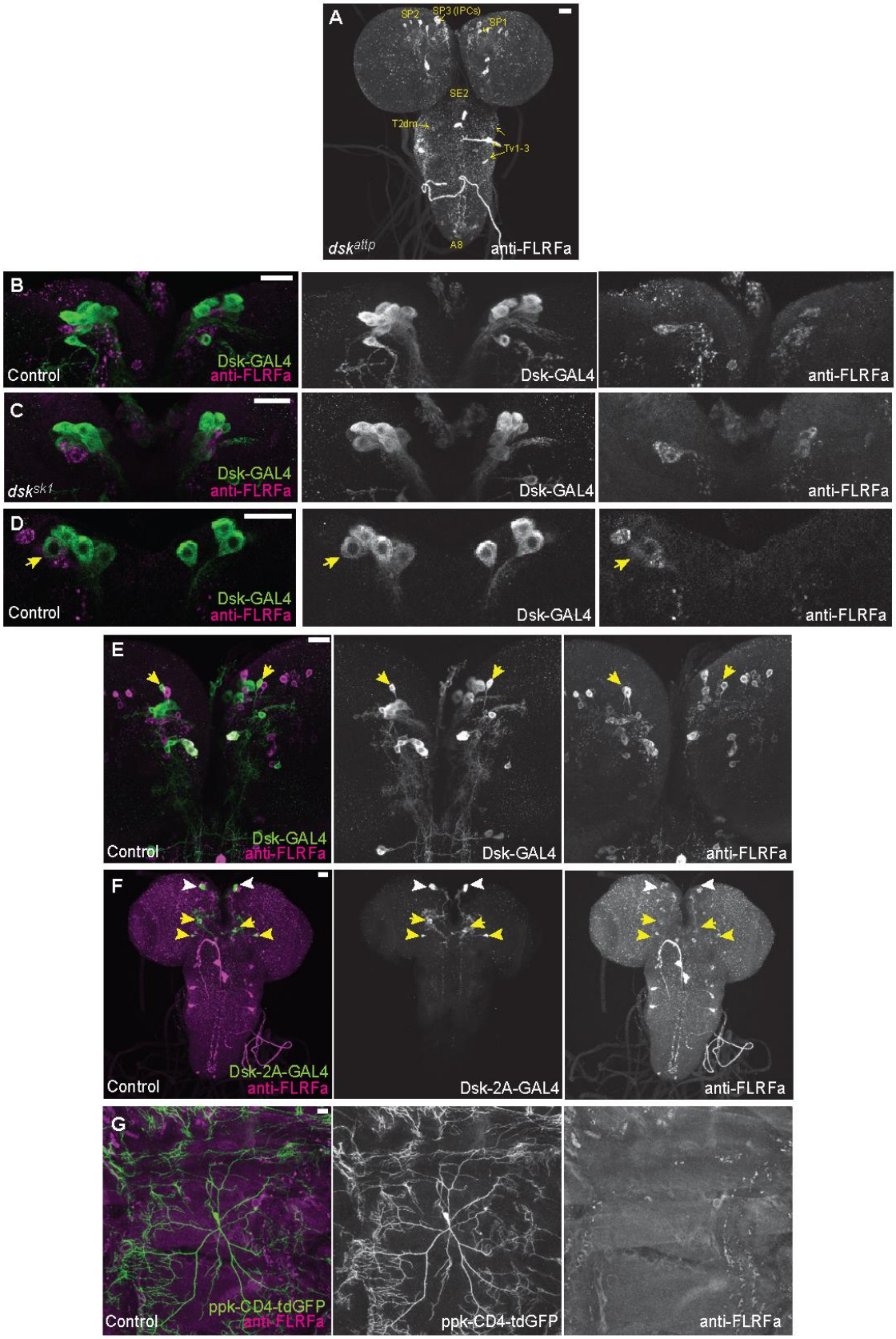
A
SP2
SP3 (IPCs)
SP1
SE2
T2dm
Tv1-3
A8
dskattp
anti-FLRFa
B
Control
Dsk-GAL4
anti-FLRFa
Dsk-GAL4
anti-FLRFa
C
dsksk1
Dsk-GAL4
anti-FLRFa
Dsk-GAL4
anti-FLRFa
D
Control
Dsk-GAL4
anti-FLRFa
Dsk-GAL4
anti-FLRFa
E
Control
Dsk-GAL4
anti-FLRFa
Dsk-GAL4
anti-FLRFa
F
Control
Dsk-2A-GAL4
anti-FLRFa
Dsk-2A-GAL4
anti-FLRFa
G
Control
ppk-CD4-tdGFP
anti-FLRFa
ppk-CD4-tdGFP
anti-FLRFa

543

Fig. S2. DSK expressions in the other brain neurons and peripheral sensory neurons (related to Fig. 2)

(A) Representative image showing staining of anti-FLRFa in *dsk*^{attp} mutants. The staining patterns were indistinguishable from *dsk*^{sk1} mutants. (B) Representative image showing staining patterns of *DSK-GAL4* and anti-FLRFa in the wild-type larval IPCs. In the wild-type brain, typically 4 to 7 IPCs are visualized by *DSK-GAL4* and 1 to 3 by anti-FLRFa consistently to the previous study by Soderberg et al.[49] that used anti-DSK raised by Nichols et al.[47] In contrast, few IPCs co-labelled were found, which is also somewhat consistent with the variability of DSK immunostaining in IPCs reported by the previous study[49]. (C) Representative image showing staining patterns of *DSK-GAL4* and anti-FLRFa in the *dsk*^{sk1} larval IPCs. Comparable staining patterns of *DSK-GAL4* and anti-FLRFa were observed in the mutant IPCs. (D) An example of rare IPC that was co-labeled by *DSK-GAL4* and anti-FLRFa in the wild-type brain (arrow). (E) Representative image showing SP1 neurons (arrows) that were rarely co-labeled by *DSK-GAL4* and anti-FLRFa. Note that faint anti-FLRFa staining was only detected in the SP1 neuron in the right hemisphere. (F) An example image showing *DSK-2A-GAL4* expression in IPCs (white arrowheads), MP1 (yellow arrows), and Sv neurons (yellow arrowheads). (G) Representative image showing double-labeling of Class IV md neurons (*ppk-CD4::tdGFP*) and anti-FLRFa staining in the dorsal larval body wall. All scale bars represent 20 µm.

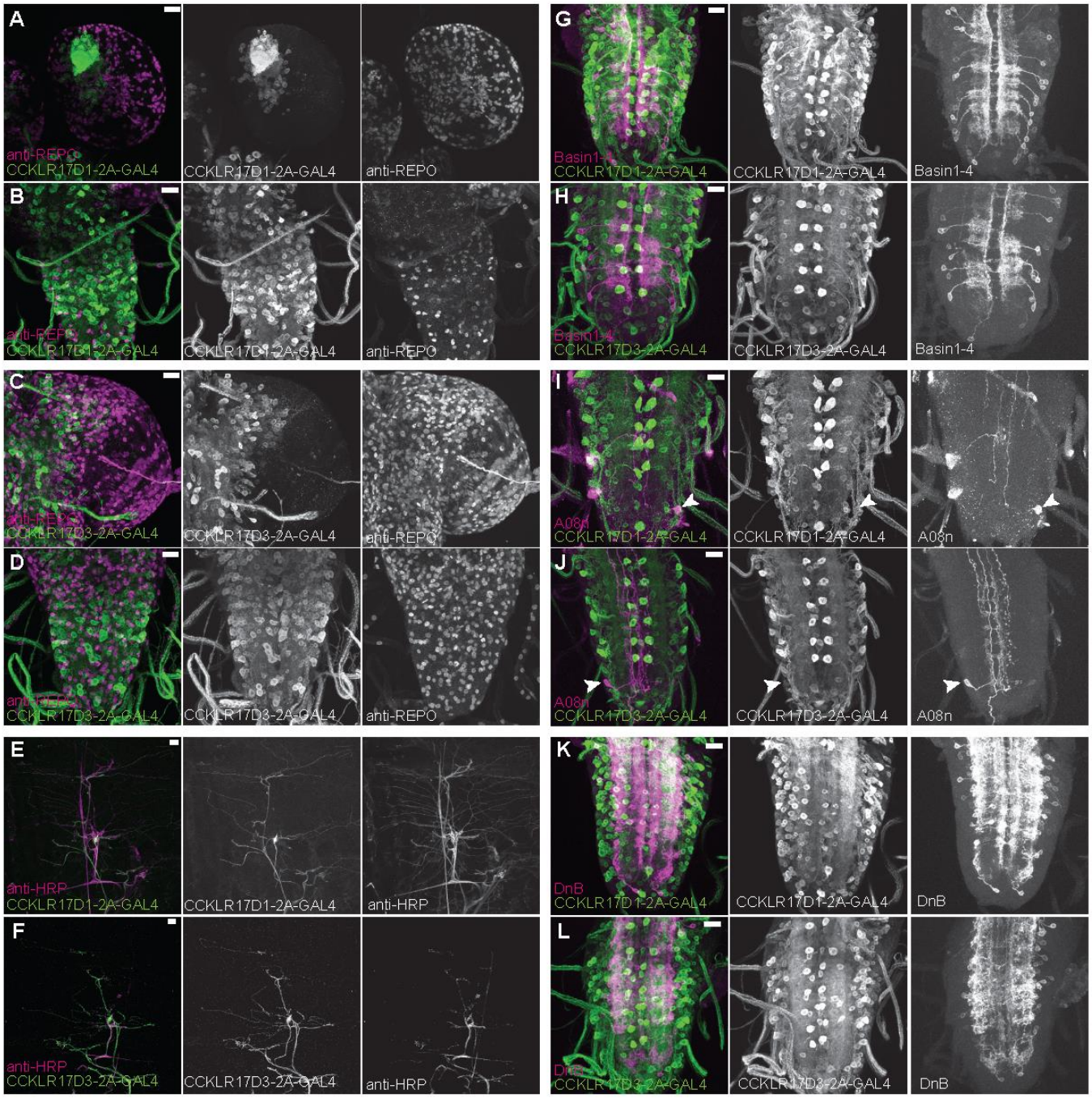
A
anti-REPO
CCKLR17D1-2A-GAL4
CCKLR17D1-2A-GAL4
anti-REPO
B
anti-REPO
CCKLR17D1-2A-GAL4
CCKLR17D1-2A-GAL4
anti-REPO
C
anti-REPO
CCKLR17D3-2A-GAL4
CCKLR17D3-2A-GAL4
anti-REPO
D
anti-REPO
CCKLR17D3-2A-GAL4
CCKLR17D3-2A-GAL4
anti-REPO
E
anti-HRP
CCKLR17D1-2A-GAL4
CCKLR17D1-2A-GAL4
anti-HRP
F
anti-HRP
CCKLR17D3-2A-GAL4
CCKLR17D3-2A-GAL4
anti-HRP
G
Basin1-4
CCKLR17D1-2A-GAL4
CCKLR17D1-2A-GAL4
Basin1-4
H
Basin1-4
CCKLR17D3-2A-GAL4
CCKLR17D3-2A-GAL4
Basin1-4
I
A08n
CCKLR17D1-2A-GAL4
CCKLR17D1-2A-GAL4
A08n
J
A08n
CCKLR17D3-2A-GAL4
CCKLR17D3-2A-GAL4
A08n
K
DnB
CCKLR17D1-2A-GAL4
CCKLR17D1-2A-GAL4
DnB
L
DnB
CCKLR17D3-2A-GAL4
CCKLR17D3-2A-GAL4
DnB

558

Fig. S3. Expression patterns of DSK receptors in larval glial cells, peripheral tissue, and nociceptive interneurons (related to Fig. 3).

(A and B) Representative images showing double-labeling of *CCKLR-17D1-T2A-GAL4* and a glial cell marker anti-REPO in the larval brain (A) and the larval VNC (B), representing little expressions of *CCKLR-17D1-T2A-GAL4* in glial cells. (C and D) Representative images showing double-labeling of *CCKLR-17D3-T2A-GAL4* and a glial cell marker anti-REPO in the larval brain (C) and in the larval VNC (D), representing little expressions of *CCKLR-17D3-T2A-GAL4* in glial cells. (E and F) Representative images showing the expressions of *CCKLR-17D1-T2A-GAL4* (E) and *CCKLR-17D3-T2A-GAL4* (F) with a peripheral neuronal marker anti-HRP in the larval body wall, showing the absence of both GAL4s from peripheral sensory neurons other than es cells. (G and H) Expressions of *CCKLR-17D1-T2A-GAL4* (G) and *CCKLR-17D3-T2A-GAL4* (H) were negligible in Basin1 to 4 neurons labeled by *R72F11-lexA* in the larval VNC. (I and J) Negligible expression of *CCKLR-17D1-T2A-GAL4* (I) and *CCKLR-17D3-T2A-GAL4* (J) found in A08n neurons labeled by *R82E12-lexA* (arrowheads) in the larval VNC. (K and L) Expressions of *CCKLR-17D1-T2A-GAL4* (K) and *CCKLR-17D3-T2A-GAL4* (L) were negligible in DnB neurons labeled by *R70F01-lexA* in the larval VNC. All scale bars represent 20 μm.

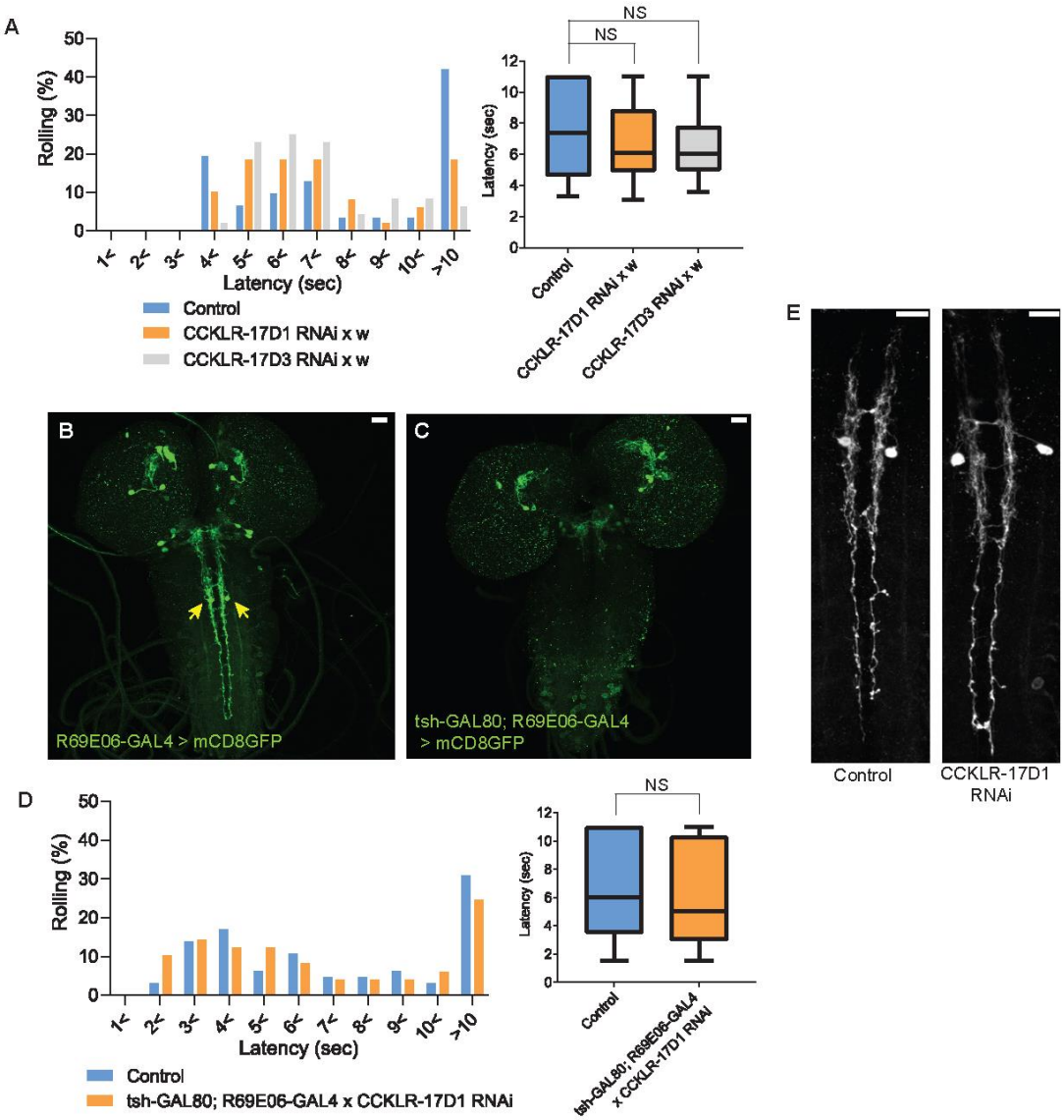

Fig. S4. CCKLR-17D1 RNAi in Goro neurons induces thermal hypersensitivity in a GAL4-dependent manner, without affecting the morphology (related to Fig. 4 and 5)

(A) Without the GAL4 driver, UAS-CCKLR-17D1 RNAi (*yv;JF02644* x w^{1118}, n = 49) and UAS-CCKLR-17D3 RNAi (*yv;JF02968* x w^{1118}, n = 48) both did not cause thermal hypersensitivity to 42 °C compared with the control (*R69E06-GAL4* x *yv; attp2*, n = 31). p > 0.38 Steel's test. (B and C) *tsh-GAL80* eliminates the expression of *R69E06-*

GAL4 from Goro neurons. The expression of *R69E06-GAL4* in Goro neurons (B) (*10xUAS-IVS-mCD8GFP; R69E06-GAL4* x *yv; attp2*) was eliminated when *tsh-GAL80* was combined with *R69E06-GAL4* (C) (*tsh-GAL80; R69E06-GAL4* x *40xUAS-IVS-mCD8GFP*). (D) When the expression of UAS-CCKLR-17D1 RNAi was eliminated from Goro neurons (*tsh-GAL80; R69E06-GAL4* x *yv; JF02644*, n = 49), larval nociceptive responses to a 42 °C probe was indistinguishable from the control (*R69E06-GAL4* x *yv; attp2*, n = 65). $p > 0.33$ Mann-Whitney's U-test. (E) Goro neurons expressing CCKLR-17D1 RNAi (*10xUAS-IVS-mCD8GFP; R69E06-GAL4* x *yv; JF02644*) did not alter their number, position, and gross projection patterns in comparison with the control (*10xUAS-IVS-mCD8GFP; R69E06-GAL4* x *yv; attp2*). All scale bars represent 20 µm. All box plots show median (middle line) and 25th to 75th percentiles with whiskers indicating the smallest to the largest data points.

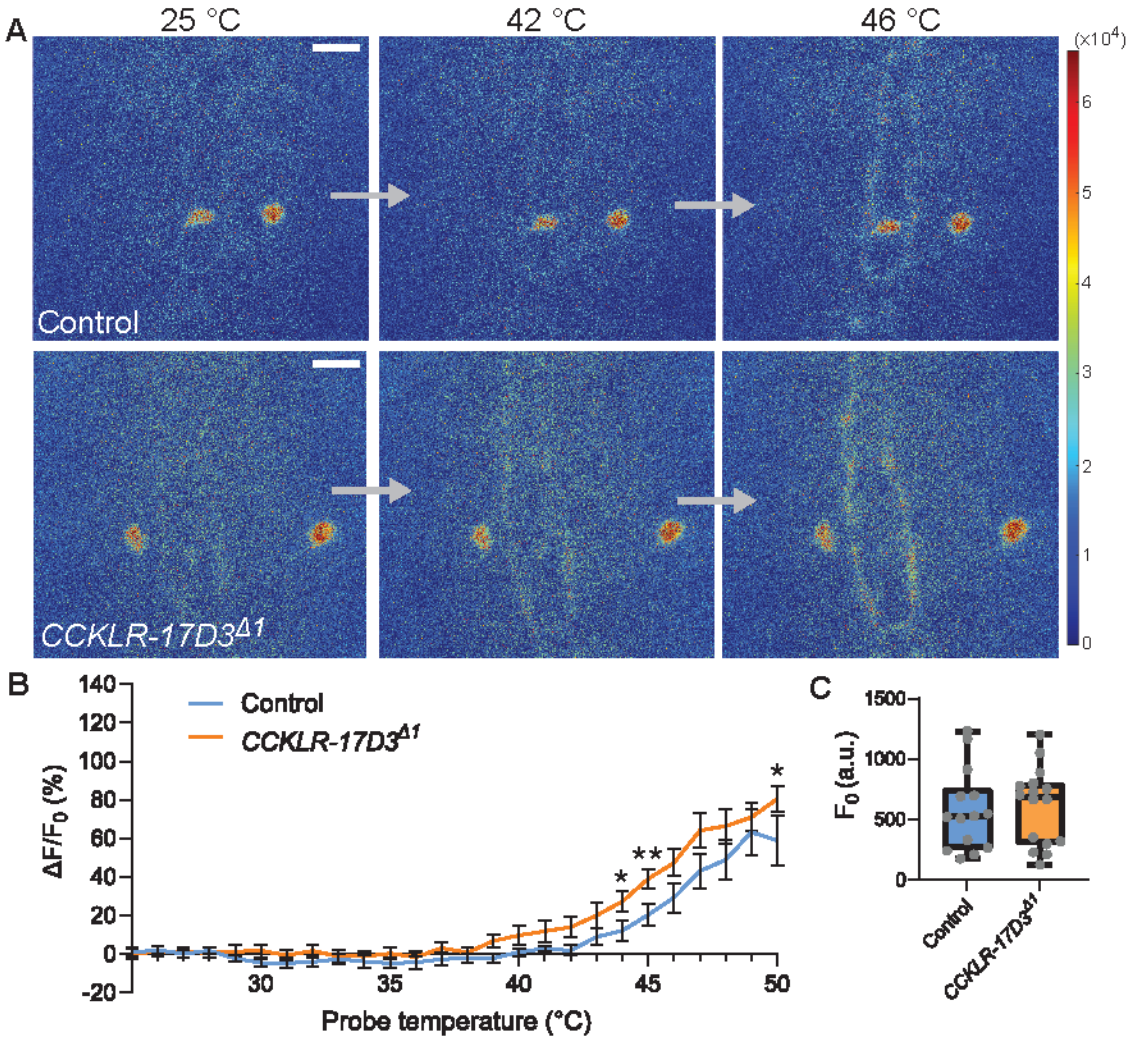

588

589 **Fig. S5. Thermal responsiveness of Goro neurons in *CCKLR-17D3$^{\Delta 1}$* (related to Fig. 5)**

590 (A) Representative still images showing thermal activation of Goro neurons in control animals (top, *yw*/Y; *R69E06-*

591 *GAL4 UAS-GCaMP6m*/+) and *CCKLR-17D3$^{\Delta 1}$* mutants (bottom, *CCKLR-17D3$^{\Delta 1}$/Y; R69E06-GAL4 UAS-*

592 *GCaMP6m*/+). See also Movie S5 and S6. Scale bars represent 20 µm. (B) Average percent increase of GCaMP6m

593 fluorescence intensity relative to baseline ($\Delta F/F_0$) during heat ramp stimulations in *CCKLR-17D3$^{\Delta 1}$* experiments.

594 $\Delta F/F_0$ is plotted to binned probe temperature (interval = 1 °C). In comparison with controls, Goro neurons of

CCKLR-17D3$^{\Delta 1}$ exhibited mildly elevated fluorescent increase of GCaMP6m, which reached statistical significance only at 44°C, 45°C, and 50°C. n = 14 and 16 for controls and *CCKLR-17D3*$^{\Delta 1}$, respectively. * $p < 0.05$, ** $p < 0.01$ (Mann–Whitney's U-test). Error bars represent standard errors. (C) Basal GCaMP6m signal levels (F_0) did not differ between controls and *CCKLR-17D3*$^{\Delta 1}$ (n = 14 and 16). $p > 0.5$ (Mann–Whitney's U-test). Box plots show median (middle line) and 25th to 75th percentiles with whiskers indicating the smallest to the largest data points.

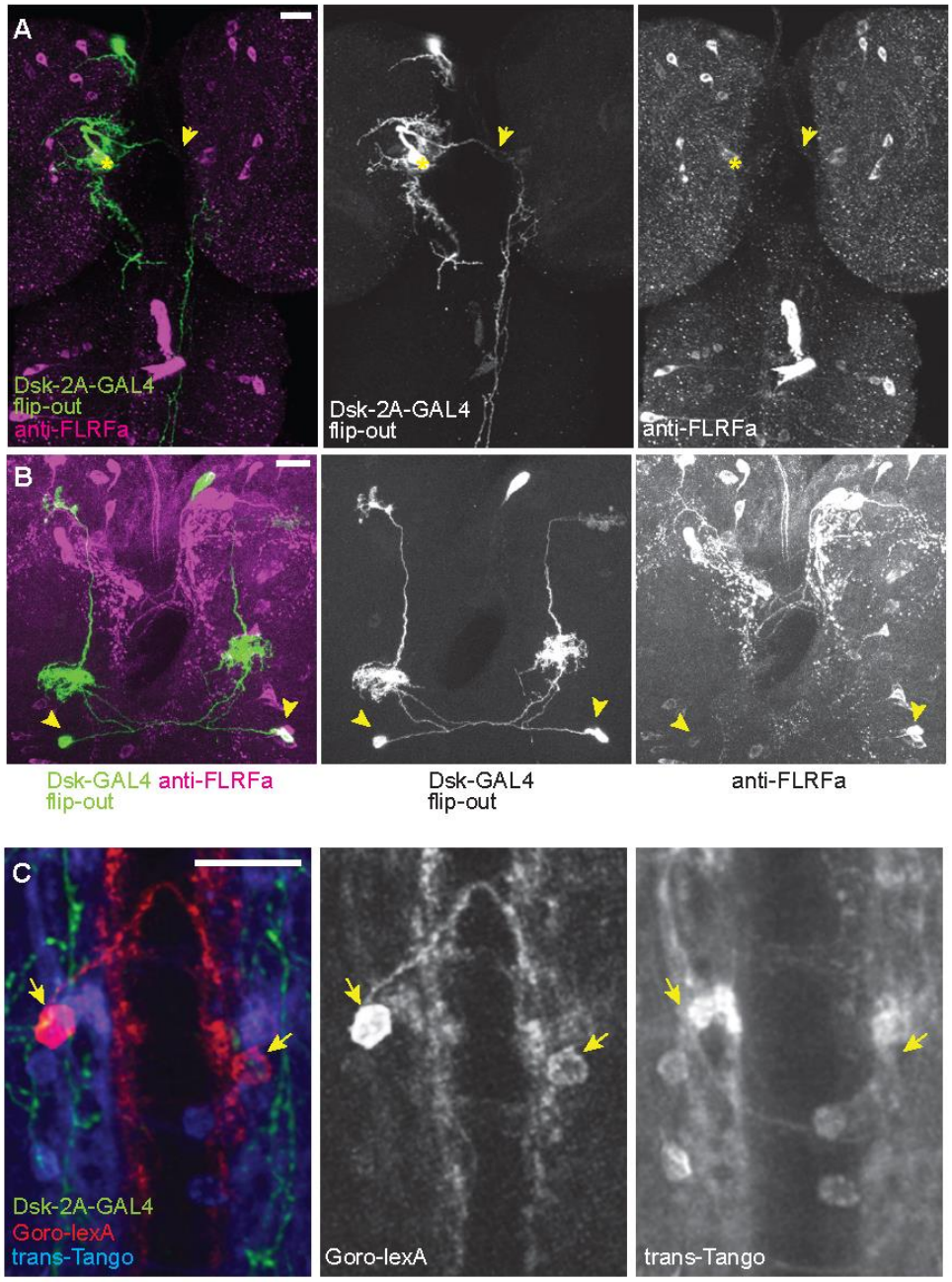

Fig. S6.Characterizations of anatomy and connectivity of DSK-expressing neurons (related to Fig. 6)

(A) Image showing a single FLP-out clone of MP1 neuron in *DSK-2A-GAL4* neurons. A commissural axon crosses the midline (arrow) and projects contra-laterally to the VNC. The asterisk indicates the soma of the MP1 neuron.

(B) Image showing two FLP-out clones of Sv neurons (arrowheads) sending ascending axons to both sides of the brain. (C) Representative image showing *trans*-Tango experiments using *DSK-2A-GAL4* (*R69E06-lexA, lexAop-rCD2::RFP UAS-mCD8::GFP; DSK-2A-GAL4* x *UAS-myrGFP, QUAS-mtdTomato::3xHA; trans-Tango*). Transsynaptic activation of Tango signals (Blue; mtdTomato::3xHA detected by anti-HA) was undetectable in Goro neurons (Red; rCD2::RFP detected by anti-CD2). Green represents MP1 axons labeled by *DSK-2A-GAL4* (myrGFP and mCD8::GFP detected by anti-GFP). Signals of mtdTom::3xHA were not detected in Goro neurons of all examined samples (n = 4). Arrows indicate Goro somata. All scale bars represent 20 µm.

Movie S1.

Ca^{2+} imaging of Goro neurons in a control animal used for the *CCKLR-17D1*$^{\Delta 1}$ experiments. See also Fig. 5. The movie was generated from heat-mapped time-series projection images of GCaMP6m fluorescence using MATLAB. Time and probe temperature are indicated at the top left and top right corners, respectively.

Movie S2.

Ca^{2+} imaging of Goro neurons in a *CCKLR-17D1*$^{\Delta 1}$ mutant animal. See also Fig. 5. The movie was generated from heat-mapped time-series projection images of GCaMP6m fluorescence using MATLAB. Time and probe temperature are indicated at the top left and top right corners, respectively.

Movie S3.

Ca^{2+} imaging of Goro neurons in a control animal used for the CCKLR-17D1 RNAi experiments. See also Fig. 5. The movie was generated from heat-mapped time-series projection images of GCaMP6m fluorescence using MATLAB. Time and probe temperature are indicated at the top left and top right corners, respectively.

Movie S4.

Ca^{2+} imaging of Goro neurons in a CCKLR-17D1 RNAi animal. See also Fig. 5. The movie was generated from heat-mapped time-series projection images of GCaMP6m fluorescence using MATLAB. Time and probe

temperature are indicated at the top left and top right corners, respectively.

Movie S5.

Ca^{2+} imaging of Goro neurons in a control animal used for the *CCKLR-17D3*$^{\Delta 1}$ experiments. See also Fig. S5. The movie was generated from heat-mapped time-series projection images of GCaMP6m fluorescence using MATLAB. Time and probe temperature are indicated at the top left and top right corners, respectively.

Movie S6.

Ca^{2+} imaging of Goro neurons in a *CCKLR-17D3*$^{\Delta 1}$ mutant animal. See also Fig. S5. The movie was generated from heat-mapped time-series projection images of GCaMP6m fluorescence using MATLAB. Time and probe temperature are indicated at the top left and top right corners, respectively.

References

1. Dubin, A.E., and Patapoutian, A. (2010). Nociceptors: the sensors of the pain pathway. J Clin Invest *120*, 3760-3772.
2. Burrell, B.D. (2017). Comparative biology of pain: What invertebrates can tell us about how nociception works. J Neurophysiol *117*, 1461-1473.
3. Walters, E.T. (2018). Nociceptive Biology of Molluscs and Arthropods: Evolutionary Clues About Functions and Mechanisms Potentially Related to Pain. Front Physiol *9*, 1049.
4. Reynolds, D.V. (1969). Surgery in the rat during electrical analgesia induced by focal brain stimulation. Science *164*, 444-445.
5. Chen, Q., and Heinricher, M.M. (2019). Descending Control Mechanisms and Chronic Pain. Current rheumatology reports *21*, 13.
6. Ossipov, M.H., Morimura, K., and Porreca, F. (2014). Descending pain modulation and chronification of pain. Curr Opin Support Palliat Care *8*, 143-151.
7. Arenas, O.M., Zaharieva, E.E., Para, A., Vasquez-Doorman, C., Petersen, C.P., and Gallio, M. (2017). Activation of planarian TRPA1 by reactive oxygen species reveals a conserved mechanism for animal nociception. Nat Neurosci *20*, 1686-1693.
8. Sneddon, L.U. (2018). Comparative Physiology of Nociception and Pain. Physiology (Bethesda) *33*, 63-73.
9. Ossipov, M.H., Dussor, G.O., and Porreca, F. (2010). Central modulation of pain. J Clin Invest *120*, 3779-

3787.

10. Heinricher, M.M., and Neubert, M.J. (2004). Neural basis for the hyperalgesic action of cholecystokinin in the rostral ventromedial medulla. J Neurophysiol *92*, 1982-1989.

11. Heinricher, M.M., McGaraughty, S., and Tortorici, V. (2001). Circuitry underlying antiopioid actions of cholecystokinin within the rostral ventromedial medulla. J Neurophysiol *85*, 280-286.

12. Marshall, T.M., Herman, D.S., Largent-Milnes, T.M., Badghisi, H., Zuber, K., Holt, S.C., Lai, J., Porreca, F., and Vanderah, T.W. (2012). Activation of descending pain-facilitatory pathways from the rostral ventromedial medulla by cholecystokinin elicits release of prostaglandin-E(2) in the spinal cord. Pain *153*, 86-94.

13. Xie, J.Y., Herman, D.S., Stiller, C.O., Gardell, L.R., Ossipov, M.H., Lai, J., Porreca, F., and Vanderah, T.W. (2005). Cholecystokinin in the rostral ventromedial medulla mediates opioid-induced hyperalgesia and antinociceptive tolerance. J Neurosci *25*, 409-416.

14. Roca-Lapirot, O., Fossat, P., Ma, S., Egron, K., Trigilio, G., Lopez-Gonzalez, M.J., Covita, J., Bouali-Benazzouz, R., Favereaux, A., Gundlach, A.L., et al. (2019). Acquisition of analgesic properties by the cholecystokinin (CCK)/CCK2 receptor system within the amygdala in a persistent inflammatory pain condition. Pain *160*, 345-357.

15. Manai, M., van Middendorp, H., Veldhuijzen, D.S., Huizinga, T.W.J., and Evers, A.W.M. (2019). How to prevent, minimize, or extinguish nocebo effects in pain: a narrative review on mechanisms, predictors, and

interventions. Pain reports *4*, e699.

16. Elphick, M.R., Mirabeau, O., and Larhammar, D. (2018). Evolution of neuropeptide signalling systems. J Exp Biol *221*.

17. Mirabeau, O., and Joly, J.S. (2013). Molecular evolution of peptidergic signaling systems in bilaterians. Proc Natl Acad Sci U S A *110*, E2028-2037.

18. Jekely, G. (2013). Global view of the evolution and diversity of metazoan neuropeptide signaling. Proc Natl Acad Sci U S A *110*, 8702-8707.

19. Nassel, D.R., and Williams, M.J. (2014). Cholecystokinin-Like Peptide (DSK) in Drosophila, Not Only for Satiety Signaling. Front Endocrinol (Lausanne) *5*, 219.

20. Tinoco, A.B., Barreiro-Iglesias, A., Yanez Guerra, L.A., Delroisse, J., Zhang, Y., Gunner, E.F., Zampronio, C.G., Jones, A.M., Egertova, M., and Elphick, M.R. (2021). Ancient role of sulfakinin/cholecystokinin-type signalling in inhibitory regulation of feeding processes revealed in an echinoderm. eLife *10*.

21. Wu, S., Guo, C., Zhao, H., Sun, M., Chen, J., Han, C., Peng, Q., Qiao, H., Peng, P., Liu, Y., et al. (2019). Drosulfakinin signaling in fruitless circuitry antagonizes P1 neurons to regulate sexual arousal in Drosophila. Nat Commun *10*, 4770.

22. Wu, F., Deng, B., Xiao, N., Wang, T., Li, Y., Wang, R., Shi, K., Luo, D.G., Rao, Y., and Zhou, C. (2020). A neuropeptide regulates fighting behavior in Drosophila melanogaster. eLife *9*.

23. Mohammad, F., Aryal, S., Ho, J., Stewart, J.C., Norman, N.A., Tan, T.L., Eisaka, A., and Claridge-Chang,

A. (2016). Ancient Anxiety Pathways Influence Drosophila Defense Behaviors. Curr Biol *26*, 981-986.

24. Tracey, W.D., Jr., Wilson, R.I., Laurent, G., and Benzer, S. (2003). painless, a Drosophila gene essential for nociception. Cell *113*, 261-273.

25. Hwang, R.Y., Zhong, L., Xu, Y., Johnson, T., Zhang, F., Deisseroth, K., and Tracey, W.D. (2007). Nociceptive neurons protect Drosophila larvae from parasitoid wasps. Curr Biol *17*, 2105-2116.

26. Zhong, L., Bellemer, A., Yan, H., Honjo, K., Robertson, J., Hwang, R.Y., Pitt, G.S., and Tracey, W.D. (2012). Thermosensory and non-thermosensory isoforms of Drosophila melanogaster TRPA1 reveal heat sensor domains of a thermoTRP channel. Cell Rep *1*, 43-55.

27. Kim, S.E., Coste, B., Chadha, A., Cook, B., and Patapoutian, A. (2012). The role of Drosophila Piezo in mechanical nociception. Nature *483*, 209-212.

28. Zhong, L., Hwang, R.Y., and Tracey, W.D. (2010). Pickpocket is a DEG/ENaC protein required for mechanical nociception in Drosophila larvae. Curr Biol *20*, 429-434.

29. Mauthner, S.E., Hwang, R.Y., Lewis, A.H., Xiao, Q., Tsubouchi, A., Wang, Y., Honjo, K., Skene, J.H., Grandl, J., and Tracey, W.D., Jr. (2014). Balboa binds to pickpocket in vivo and is required for mechanical nociception in Drosophila larvae. Curr Biol *24*, 2920-2925.

30. Babcock, D.T., Shi, S., Jo, J., Shaw, M., Gutstein, H.B., and Galko, M.J. (2011). Hedgehog signaling regulates nociceptive sensitization. Curr Biol *21*, 1525-1533.

31. Honjo, K., Mauthner, S.E., Wang, Y., Skene, J.H., and Tracey, W.D., Jr. (2016). Nociceptor-Enriched Genes

Required for Normal Thermal Nociception. Cell Rep *16*, 295-303.

32. Honjo, K., and Tracey, W.D., Jr. (2018). BMP signaling downstream of the Highwire E3 ligase sensitizes nociceptors. PLoS Genet *14*, e1007464.

33. Neely, G.G., Hess, A., Costigan, M., Keene, A.C., Goulas, S., Langeslag, M., Griffin, R.S., Belfer, I., Dai, F., Smith, S.B., et al. (2010). A genome-wide Drosophila screen for heat nociception identifies alpha2delta3 as an evolutionarily conserved pain gene. Cell *143*, 628-638.

34. Follansbee, T.L., Gjelsvik, K.J., Brann, C.L., McParland, A.L., Longhurst, C.A., Galko, M.J., and Ganter, G.K. (2017). Drosophila Nociceptive Sensitization Requires BMP Signaling via the Canonical SMAD Pathway. J Neurosci *37*, 8524-8533.

35. Burgos, A., Honjo, K., Ohyama, T., Qian, C.S., Shin, G.J., Gohl, D.M., Silies, M., Tracey, W.D., Zlatic, M., Cardona, A., et al. (2018). Nociceptive interneurons control modular motor pathways to promote escape behavior in Drosophila. eLife *7*.

36. Kaneko, T., Macara, A.M., Li, R., Hu, Y., Iwasaki, K., Dunnings, Z., Firestone, E., Horvatic, S., Guntur, A., Shafer, O.T., et al. (2017). Serotonergic Modulation Enables Pathway-Specific Plasticity in a Developing Sensory Circuit in Drosophila. Neuron *95*, 623-638 e624.

37. Takagi, S., Cocanougher, B.T., Niki, S., Miyamoto, D., Kohsaka, H., Kazama, H., Fetter, R.D., Truman, J.W., Zlatic, M., Cardona, A., et al. (2017). Divergent Connectivity of Homologous Command-like Neurons Mediates Segment-Specific Touch Responses in Drosophila. Neuron *96*, 1373-1387 e1376.

38. Dason, J.S., Cheung, A., Anreiter, I., Montemurri, V.A., Allen, A.M., and Sokolowski, M.B. (2020). Drosophila melanogaster foraging regulates a nociceptive-like escape behavior through a developmentally plastic sensory circuit. Proc Natl Acad Sci U S A *117*, 23286-23291.

39. Hu, Y., Wang, C., Yang, L., Pan, G., Liu, H., Yu, G., and Ye, B. (2020). A Neural Basis for Categorizing Sensory Stimuli to Enhance Decision Accuracy. Curr Biol *30*, 4896-4909 e4896.

40. Chin, M.R., and Tracey, W.D., Jr. (2017). Nociceptive Circuits: Can't Escape Detection. Curr Biol *27*, R796-R798.

41. Hu, C., Petersen, M., Hoyer, N., Spitzweck, B., Tenedini, F., Wang, D., Gruschka, A., Burchardt, L.S., Szpotowicz, E., Schweizer, M., et al. (2017). Sensory integration and neuromodulatory feedback facilitate Drosophila mechanonociceptive behavior. Nat Neurosci *20*, 1085-1095.

42. Im, S.H., Takle, K., Jo, J., Babcock, D.T., Ma, Z., Xiang, Y., and Galko, M.J. (2015). Tachykinin acts upstream of autocrine Hedgehog signaling during nociceptive sensitization in Drosophila. eLife *4*, e10735.

43. Bachtel, N.D., Hovsepian, G.A., Nixon, D.F., and Eleftherianos, I. (2018). Allatostatin C modulates nociception and immunity in Drosophila. Scientific reports *8*, 7501.

44. Aldrich, B.T., Kasuya, J., Faron, M., Ishimoto, H., and Kitamoto, T. (2010). The amnesiac gene is involved in the regulation of thermal nociception in Drosophila melanogaster. J Neurogenet *24*, 33-41.

45. Chen, X., Peterson, J., Nachman, R.J., and Ganetzky, B. (2012). Drosulfakinin activates CCKLR-17D1 and promotes larval locomotion and escape response in Drosophila. Fly (Austin) *6*, 290-297.

46. Kubiak, T.M., Larsen, M.J., Burton, K.J., Bannow, C.A., Martin, R.A., Zantello, M.R., and Lowery, D.E. (2002). Cloning and functional expression of the first Drosophila melanogaster sulfakinin receptor DSK-R1. Biochem Biophys Res Commun *291*, 313-320.

47. Nichols, R., and Lim, I.A. (1996). Spatial and temporal immunocytochemical analysis of drosulfakinin (Dsk) gene products in the Drosophila melanogaster central nervous system. Cell Tissue Res *283*, 107-116.

48. Veenstra, J.A., Agricola, H.J., and Sellami, A. (2008). Regulatory peptides in fruit fly midgut. Cell Tissue Res *334*, 499-516.

49. Soderberg, J.A., Carlsson, M.A., and Nassel, D.R. (2012). Insulin-Producing Cells in the Drosophila Brain also Express Satiety-Inducing Cholecystokinin-Like Peptide, Drosulfakinin. Front Endocrinol (Lausanne) *3*, 109.

50. Park, D., Veenstra, J.A., Park, J.H., and Taghert, P.H. (2008). Mapping peptidergic cells in Drosophila: where DIMM fits in. PLoS One *3*, e1896.

51. Nassel, D.R., and Winther, A.M. (2010). Drosophila neuropeptides in regulation of physiology and behavior. Prog Neurobiol *92*, 42-104.

52. Ohyama, T., Schneider-Mizell, C.M., Fetter, R.D., Aleman, J.V., Franconville, R., Rivera-Alba, M., Mensh, B.D., Branson, K.M., Simpson, J.H., Truman, J.W., et al. (2015). A multilevel multimodal circuit enhances action selection in Drosophila. Nature *520*, 633-639.

53. van den Pol, A.N. (2012). Neuropeptide transmission in brain circuits. Neuron *76*, 98-115.

54. Fuxe, K., Borroto-Escuela, D.O., Romero-Fernandez, W., Zhang, W.B., and Agnati, L.F. (2013). Volume transmission and its different forms in the central nervous system. Chinese journal of integrative medicine *19*, 323-329.

55. Nicolai, L.J., Ramaekers, A., Raemaekers, T., Drozdzecki, A., Mauss, A.S., Yan, J., Landgraf, M., Annaert, W., and Hassan, B.A. (2010). Genetically encoded dendritic marker sheds light on neuronal connectivity in Drosophila. Proc Natl Acad Sci U S A *107*, 20553-20558.

56. Hamada, F.N., Rosenzweig, M., Kang, K., Pulver, S.R., Ghezzi, A., Jegla, T.J., and Garrity, P.A. (2008). An internal thermal sensor controlling temperature preference in Drosophila. Nature *454*, 217-220.

57. Feinberg, E.H., Vanhoven, M.K., Bendesky, A., Wang, G., Fetter, R.D., Shen, K., and Bargmann, C.I. (2008). GFP Reconstitution Across Synaptic Partners (GRASP) defines cell contacts and synapses in living nervous systems. Neuron *57*, 353-363.

58. Gordon, M.D., and Scott, K. (2009). Motor control in a Drosophila taste circuit. Neuron *61*, 373-384.

59. Roy, S., Huang, H., Liu, S., and Kornberg, T.B. (2014). Cytoneme-mediated contact-dependent transport of the Drosophila decapentaplegic signaling protein. Science *343*, 1244624.

60. Gonzalez-Mendez, L., Seijo-Barandiaran, I., and Guerrero, I. (2017). Cytoneme-mediated cell-cell contacts for Hedgehog reception. eLife *6*.

61. Macpherson, L.J., Zaharieva, E.E., Kearney, P.J., Alpert, M.H., Lin, T.Y., Turan, Z., Lee, C.H., and Gallio, M. (2015). Dynamic labelling of neural connections in multiple colours by trans-synaptic fluorescence

complementation. Nat Commun *6*, 10024.

62. Talay, M., Richman, E.B., Snell, N.J., Hartmann, G.G., Fisher, J.D., Sorkac, A., Santoyo, J.F., Chou-Freed, C., Nair, N., Johnson, M., et al. (2017). Transsynaptic Mapping of Second-Order Taste Neurons in Flies by trans-Tango. Neuron *96*, 783-795 e784.

63. Chen, X., and Ganetzky, B. (2012). A neuropeptide signaling pathway regulates synaptic growth in Drosophila. J Cell Biol *196*, 529-543.

64. Im, S.H., Patel, A.A., Cox, D.N., and Galko, M.J. (2018). Drosophila Insulin receptor regulates the persistence of injury-induced nociceptive sensitization. Dis Model Mech *11*.

65. Pommier, B., Beslot, F., Simon, A., Pophillat, M., Matsui, T., Dauge, V., Roques, B.P., and Noble, F. (2002). Deletion of CCK2 receptor in mice results in an upregulation of the endogenous opioid system. J Neurosci *22*, 2005-2011.

66. Noble, F., and Roques, B.P. (2002). Phenotypes of mice with invalidation of cholecystokinin (CCK(1) or CCK(2)) receptors. Neuropeptides *36*, 157-170.

67. Baber, N.S., Dourish, C.T., and Hill, D.R. (1989). The role of CCK caerulein, and CCK antagonists in nociception. Pain *39*, 307-328.

68. Suh, H.H., and Tseng, L.F. (1990). Differential effects of sulfated cholecystokinin octapeptide and proglumide injected intrathecally on antinociception induced by beta-endorphin and morphine administered intracerebroventricularly in mice. Eur J Pharmacol *179*, 329-338.

69. Liu, Y., Latremoliere, A., Li, X., Zhang, Z., Chen, M., Wang, X., Fang, C., Zhu, J., Alexandre, C., Gao, Z., et al. (2018). Touch and tactile neuropathic pain sensitivity are set by corticospinal projections. Nature *561*, 547-550.

70. Curtright, A., Rosser, M., Goh, S., Keown, B., Wagner, E., Sharifi, J., Raible, D.W., and Dhaka, A. (2015). Modeling Nociception in Zebrafish: A Way Forward for Unbiased Analgesic Discovery. Plos One *10*.

71. Milinkeviciute, G., Gentile, C., and Neely, G.G. (2012). Drosophila as a tool for studying the conserved genetics of pain. Clinical genetics *82*, 359-366.

72. Tobin, D.M., and Bargmann, C.I. (2004). Invertebrate nociception: Behaviors, neurons and molecules. Journal of Neurobiology *61*, 161-174.

73. Malafoglia, V., Bryant, B., Raffaeli, W., Giordano, A., and Bellipanni, G. (2013). The zebrafish as a model for nociception studies. Journal of Cellular Physiology *228*, 1956-1966.

74. Khuong, T.M., Wang, Q.P., Manion, J., Oyston, L.J., Lau, M.T., Towler, H., Lin, Y.Q., and Neely, G.G. (2019). Nerve injury drives a heightened state of vigilance and neuropathic sensitization in Drosophila. Science advances *5*, eaaw4099.

75. Kondo, S., Takahashi, T., Yamagata, N., Imanishi, Y., Katow, H., Hiramatsu, S., Lynn, K., Abe, A., Kumaraswamy, A., and Tanimoto, H. (2020). Neurochemical Organization of the Drosophila Brain Visualized by Endogenously Tagged Neurotransmitter Receptors. Cell Rep *30*, 284-297 e285.

76. Wong, A.M., Wang, J.W., and Axel, R. (2002). Spatial representation of the glomerular map in the

Drosophila protocerebrum. Cell *109*, 229-241.

77. Ren, Q., Awasaki, T., Huang, Y.F., Liu, Z., and Lee, T. (2016). Cell Class-Lineage Analysis Reveals Sexually Dimorphic Lineage Compositions in the Drosophila Brain. Curr Biol *26*, 2583-2593.

78. Deng, B., Li, Q., Liu, X., Cao, Y., Li, B., Qian, Y., Xu, R., Mao, R., Zhou, E., Zhang, W., et al. (2019). Chemoconnectomics: Mapping Chemical Transmission in Drosophila. Neuron *101*, 876-893 e874.

79. Kondo, S., and Ueda, R. (2013). Highly improved gene targeting by germline-specific Cas9 expression in Drosophila. Genetics *195*, 715-721.

80. Bischof, J., Bjorklund, M., Furger, E., Schertel, C., Taipale, J., and Basler, K. (2013). A versatile platform for creating a comprehensive UAS-ORFeome library in Drosophila. Development *140*, 2434-2442.

81. Marder, E., Calabrese, R.L., Nusbaum, M.P., and Trimmer, B. (1987). Distribution and partial characterization of FMRFamide-like peptides in the stomatogastric nervous systems of the rock crab, Cancer borealis, and the spiny lobster, Panulirus interruptus. J Comp Neurol *259*, 150-163.

82. Chen, T.W., Wardill, T.J., Sun, Y., Pulver, S.R., Renninger, S.L., Baohan, A., Schreiter, E.R., Kerr, R.A., Orger, M.B., Jayaraman, V., et al. (2013). Ultrasensitive fluorescent proteins for imaging neuronal activity. Nature *499*, 295-300.

83. Feng, Y., Ueda, A., and Wu, C.F. (2004). A modified minimal hemolymph-like solution, HL3.1, for physiological recordings at the neuromuscular junctions of normal and mutant Drosophila larvae. J Neurogenet *18*, 377-402.